

Tero Kämäräinen

**Growth Kinetics and Stability of
Self-Assembled Alkylsilane
Monolayers on Cellulose Nanofibril
Films**

School of Electrical Engineering

Thesis submitted for examination for the degree of
Master of Science in Technology.

Espoo 2.10.2014

Thesis supervisor:

Prof. Harri Lipsanen

Thesis advisor:

Dr. Lokanathan Arcot

Author: Tero Kämäräinen

Title: Growth Kinetics and Stability of Self-Assembled Alkylsilane Monolayers on Cellulose Nanofibril Films

Date: 2.10.2014

Language: English

Number of pages: 6+41

Department of Micro- and Nanosciences

Professorship: Micro and Nanotechnology

Code: S3010

Supervisor: Prof. Harri Lipsanen

Advisor: Dr. Lokanathan Arcot

Paper-based microfluidic sensors are becoming very popular in applications requiring chemical analysis. This thesis deals with preliminary surface chemistry studies which form the foundation for development of cellulosic microfluidic devices. Nanocellulose was chosen as the substrate and alkylsilanes were used to modify its wetting characteristics.

The growth kinetics of alkylsilane self-assembled monolayers (SAMs) prepared on cellulose nanofibril (CNF) film was studied. The stability of the silane modification was tested in ambient environment, 50 and 100 % relative humidity, in alkaline and acidic vapour, and under 254 nm and 366 nm wavelength ultraviolet (UV) light irradiation. The SAMs were also exposed to UV light in conjunction with its associated ozone (O_3). Protein and polyelectrolyte adsorption onto native and silane-modified CNF films was investigated. Water contact angle measurements were used to characterize the wetting properties of the films, while atomic force microscopy was used to probe their surface morphology. The chemical composition of the surfaces was analysed with X-ray photoelectron spectroscopy.

The silane-modifications proved largely stable in the above environments with the exception of UV/ O_3 treatment. Hydrophilic-hydrophobic patterns were created on silane-modified CNF film using masked exposure to UV/ O_3 , which degrades the alkyl chains of silanes at the mask opening. The patterned film wetting characteristics turned out not to be applicable for fluid flow.

Keywords: nanocellulose, cellulose nanofibril, silane, hydrophobic patterns, self-assembled monolayer, growth kinetics, stability

Tekijä: Tero Kämäräinen

Työn nimi: Nanofibrilloidulle selluloosakalvolle valmistetun itsejärjestyvän alkyylisilaaniyksikerroksen kasvukinetiikka ja stabiilius

Päivämäärä: 2.10.2014

Kieli: Englanti

Sivumäärä: 6+41

Mikro- ja nanotekniikan laitos

Professori: Mikro- ja nanotekniikka

Koodi: S3010

Valvoja: Prof. Harri Lipsanen

Ohjaaja: FT Lokanathan Arcot

Paperipohjaista mikrofluidistiikkaa höydynnetään yhä enemmän kemiallista analyysia vaativissa sovelluksissa. Tämä diplomityö käsittelee alustavaa pintakemiatutkimusta, joka luo pohjaa mikrofluidistiselle selluloosapinnalle. Työn kohdepinnaksi valittiin nanoselluloosakalvo, jonka kastuvuutta muokattiin alkyylisilaaneilla.

Työssä tutkittiin nanofibrilloidulle selluloosakalvolle (engl. cellulose nanofibril, CNF) valmistetun alkyylisilaaniyksikerroksen kasvukinetiikkaa ja stabiiliutta. Stabiiliutta tutkittiin säilyttämällä silaanikäsiteltyjä CNF kalvoja laboratorioolosuhteissa, 50 ja 100 % suhteellisessa kosteudessa, emäksisessä ja happamassa höyryssä sekä altistamalla ne 254 nm ja 366 nm aallonpituiselle ultraviolettisäteilylle (UV-säteily). Myös UV-säteilyn ja otsonin yhteisvaikutusta tutkittiin. Lopuksi alkuperäisen ja silaanikäsitellyn CNF kalvon proteiinin ja polyelektrolyytin adsorptiokykyä analysoitiin. Veden kontaktikulmamittauksilla karakterisoitiin pinnan kastuvuutta. Atomivoimamikroskoopilla tutkittiin pinnan morfologiaa ja sen kemiallista koostumusta analysoitiin röntgenfotoelektronispektroskopian avulla.

CNF:n silaanikäsitely oli enimmäkseen stabiili edellä mainituissa ympäristöissä. Silaanikäsitellyn CNF kalvon kastuvuus muutettiin osittain hydrofiiliseksi altistamalla se rajoitetusti UV-säteilylle ja otsonille, mikä hajottaa silaanien hydrofobiset alkyyliketjut maskin läpinäkyviltä kohdilta. Kuvioitun silaanikäsitellyn CNF kalvon kastuvuusominaisuudet eivät sallineet sen käyttöä nestevirtauskanavana.

Avainsanat: nanoselluloosa, nanofibrilloitu selluloosa, silaani, hydrofobinen kuviointi, itsejärjestyvä yksikerros, kasvukinetiikka, stabiilius

Preface

This thesis summarises the results of the work done during my six-month employment at the Forest Products Surface Chemistry group, headed by Prof. Janne Laine, at the Aalto University School of Chemical Technology. A lot of interesting research was carried out at their facilities by many an interesting figure to which a warm acknowledgement is kindly extended in the following paragraph.

First and foremost I would like to thank Prof. Janne Laine for giving me the opportunity to work in his group whilst writing this thesis, Prof. Harri Lipsanen for taking the time for supervisory duties, and my advisor Lokanathan for his tireless and unrivalled tutelage. Many thanks to Prof. Sami Franssila and Ville Jokinen from Microfabrication group for lending UV/O₃ masks and valuable skills at our disposal. Tekla Tammelin from VTT is acknowledged for providing the nanocellulose film. Leena-Sisko Johansson and Joseph Campbell are thanked for their hard work in X-ray photoelectron spectroscopy measurements. Thanks to Juan Delgado and Maija Vuoriluoto for giving me instruction on the use of atomic force microscope. The numerous advices and help given me by the highly skilled staff of the Department of Forest Products Technology cannot be overstated and I would like to thank especially laboratory supervisors Ritva Kivelä, Rita Hatakka, Marja Kärkkäinen, and Anu Anttila.

Lastly, I feel obliged to thank my parents for their support and understanding that they have given me during the past years. In retrospect, it has not always been possible to show them gratitude to the extent that a simple rationale would warrant.

Espoo, October 2, 2014

Tero Kämäräinen

Contents

Abstract	ii
Abstract (in Finnish)	iii
Preface	iv
Contents	v
Abbreviations	vi
1 Introduction	1
2 Background	3
2.1 Paper-Based Microfluidics	3
2.2 Cellulose and Nanocellulosic Materials	5
2.3 Silane SAMs	6
2.3.1 Growth Mechanism and Kinetics	7
2.3.2 Degradation	9
2.4 Wetting and Wicking	11
2.5 Protein and Polyelectrolyte Adsorption	14
3 Experimental	16
3.1 Materials	16
3.1.1 Chemicals	16
3.1.2 CNF Film	17
3.2 Methods	17
3.2.1 UV Ozonation	17
3.2.2 SAM Growth Methods	17
3.2.3 Stability Tests	18
3.2.4 BSA and PEI Adsorption	18
3.2.5 Contact Angle Measurement	18
3.2.6 Atomic Force Microscopy	19
3.2.7 X-Ray Photoelectron Spectroscopy	20
4 Results and Discussion	22
4.1 CNF Film Characterization	22
4.2 Growth Kinetics	23
4.3 Stability	26
4.3.1 Ambient and Water Vapour	26
4.3.2 HCl and NH ₃ Vapour	29
4.3.3 UV Light and UV/O ₃	29
4.4 Patterning of SAMs via Masked UV/O ₃ Exposure	32
4.5 BSA and PEI Adsorption	32
5 Conclusions	34
References	35

Abbreviations

AA	acetic acid
AFM	atomic force microscopy
BNC	bacterial nanocellulose
BSA	bovine serum albumin
CI	confidence interval
CNC	cellulose nanocrystal
CNF	cellulose nanofibril
CPS	counts per second
HCl	hydrochloric acid
NH ₃	ammonia
O ₃	ozone
PBS	phosphate buffered saline
PEI	polyethylenimine
pI	isoelectric point
RH	relative humidity
S1	<i>n</i> -octyldimethylchlorosilane
S2	<i>n</i> -octylmethyldichlorosilane
S3	<i>n</i> -octyltrichlorosilane
S6	1,2-bis(trichlorosilyl)decane
SAM	self-assembled monolayer
UV	ultraviolet
WCA	water contact angle
XPS	X-ray photoelectron spectroscopy

1 Introduction

Environmentally sound exploitation of resources is an important ingredient in the sustained human existence on earth, while also acting as an investment in the welfare and preservation of a diverse gene pool. Such sentiment has set forth propositions to invest in green technology, as illustrated e.g. by the work of World Wide Fund for Nature (wwf.panda.org, 2014). Green technology in Aalto University manifests in its mission statement by demanding a holistic approach to sustainable development in research, teaching, and management of its property (aalto.fi, 2014). On a national level, this fits into Finland's investment in green technology as laid out in the recent decisions of the government to pursue a more environmentally friendly line (valtioneuvosto.fi, 2013), exemplified by the ongoing programmes of Tekes (Finnish Funding Agency for Technology and Innovation), which include initiatives in renewable energy and materials (tekes.fi, 2014).

Chemical analysis in developing countries, e.g. human and livestock diagnostics or monitoring of environmental hazards and food safety, poses challenges not present in urban settings due to the lack of resources and infrastructure (Yetisen et al., 2013). As a part of the overall trend in miniaturization of technology, the field of analytical chemistry has welcomed the use of microfluidic devices, which offer portability, low reagent consumption, high sensitivity, and speedy analysis (Whitesides, 2006). Although microfluidic devices now show great variety in functionality, commercially available products have been scarce (Blow, 2009). The introduction of paper-based platforms could realize the expectations of microfluidics by producing concepts of great commercial value in disposable point-of-care applications e.g. in resource-limited settings. The development of such analysis systems for biological samples is also the aim of the Microfluidics project, through which this thesis was funded. The general importance of plant-based materials have been long recognized for their merits. For instance, the most abundant biopolymer, i.e. cellulose, is natively biodegradable and exhibits good biocompatibility in addition to having a highly tunable surface chemistry (Klemm et al., 2005). Furthermore, the inherent ability of cellulose to arrange into micro- and nanosized fibrils has continued to play an important role in many of its modern applications where e.g. high specific surface area is in demand. (Klemm et al., 2011) Consequently, the research interest towards nanocelluloses has been steadily increasing (Milanez et al., 2013).

The objective of this thesis was to create hydrophilic channels on a hydrophobized nanocellulose film and to test the stability of the hydrophobic modification in various environments. More specifically, cellulose nanofibril (CNF) film surface was hydrophobized with an alkylsilane self-assembled monolayer (SAM). Four different alkylsilanes with varying number of chlorine functionalities per molecule were used to investigate whether an increase in the number of covalently bonding silanol moieties per alkyl chain translates to a more stable SAM. The stability of SAMs was tested in ambient environment, 50 % relative humidity (RH), 100 % RH, hydrochloric acid (HCl) vapour, and ammonia (NH₃) vapour. The films were also ir-

radiated with ultraviolet (UV) light. Additionally, the combined effect of UV light and ozone (O_3) was studied. Lastly, the adsorption of bovine serum albumin (BSA) and polyethylenimine (PEI) onto native and silane-modified CNF films was investigated. The chemical composition of the films was analysed with X-ray photoelectron spectroscopy (XPS), while atomic force microscopy (AFM) was used to probe changes in surface morphology. Water contact angle (WCA) measurements were used to characterize the extent of wetting of the films.

This thesis is organized as follows. Section 2 covers the background on the overall field of paper-based microfluidics, nanocellulosic materials, and the nature of the chemical modification of cellulose with silanes. Section 2 ends with a brief theoretical treatment of wetting phenomena and factors affecting the adsorption of proteins and polyelectrolytes. Section 3 contains descriptions of the materials and experimental methods used. Results of the growth kinetics, stability tests, and BSA/PEI adsorption studies are presented in Section 4. Section 5 ends this thesis with concluding remarks.

2 Background

This section covers background on paper-based microfluidics and nanocellulosic materials in general. Also, this section aims at giving a qualitative understanding of the physico-chemical processes that affect the growth of silane SAMs and their degradation in various environments. The key theoretical aspects of wetting phenomenon on solid and porous surfaces are then briefly introduced, ending with an analysis of protein and polyelectrolyte adsorption.

2.1 Paper-Based Microfluidics

In the field of microfluidics, studies are aimed at understanding the flow and control of small amounts of fluids. Extensively studied polymers, such as polydimethylsiloxane, were widely utilized in the early years of microfluidics research, at which time interest was spurred partly by developments in soft-lithographic methods. (Whitesides, 2006) Paper has become an attractive alternative to the more traditional materials in the past decade. Typical uses for diagnostics on paper that have already seen commercial use include, e.g., pregnancy and drug tests taken from urine or saliva (Klasner et al., 2010). A forte of paper-based platforms, in addition to low cost, is that even unaltered they can induce a flow of analytes without any ad hoc equipment, which makes them especially appealing as disposable point-of-care diagnostic tools (Yetisen et al., 2013). The flow is driven by capillary action generated by the intricate porous network of interfibrillar space. The overall principle of capillary driven flow can be implemented in other substrates as well by fabricating multiple thin channels at the end of the device to drive analyte into the detection zones (Juncker et al., 2002).

The modification of fibrous surfaces needs to address the issue of porosity to control fluid flow by clogging the pores physically or by creating hydrophobic barriers through chemical modification (Li et al., 2012). Existing methods to engineer the wetting of paper surfaces are manifold. For instance, photoresist application followed by curing via UV light irradiation, similar to photolithography used in semiconductor industry, has been used to this end (Martinez et al., 2008b). Some approaches use printers to introduce the reactants. In inkjet printing, minute hydrophobization agent droplets can be deposited with great precision (Li et al., 2010). Wax printing offers an alternative to inkjetting, as depositing wax can be accomplished with commercially available printers. The modification is finalized by a heat treatment which melts the wax and allows it to permeate deeper into the paper. (Carrilho et al., 2009) Alternatively, the paper itself can be cut into a channel shape (Fenton et al., 2009).

As the focus of paper-based analytical devices will be in the resource-poor settings, devices have to be designed to require minimal user intervention and the need for specialized skills. Essential components for reagent handling in channels, e.g. mixing, focusing, and dilution, can be implemented in lateral flow strips (Osborn et al.,

2010). Further increasing the functionality of lateral flow assays can be achieved through clever programming of reagent flow in two dimensions (Fu et al., 2010; Apilux et al., 2013) or by employing channel structure in multilayered platforms (see Figure 1b) (Martinez et al., 2008a). A novel approach to multistep reactions on paper is the so-called digital microfluidics, where fluid is manipulated as individual droplets by an array of electrodes, affording a different kind of control for reactions (see Figure 1c) (Fobel et al., 2014).

Perhaps reflecting the user base of point-of-care diagnostics, the formats used to produce a readable output at the detection zone have been slow to adopt quantitative analysis (Blow, 2009). Although this has not been a problem when only binary information is required, e.g., in pregnancy tests, expanding the precision of detection methods would greatly benefit this field. Currently, methods utilizing colourimetric (see Figure 1a), electrochemical, electrochemiluminescence, fluorescence, chemiluminescence, and nanoparticle-based schemes have been demonstrated on paper (Yetisen et al., 2013). The above examples illustrate the great potential in paper-based microfluidic systems, but development of existing technologies and research into alternative solutions are needed to produce applications where simplicity of user-experience and quality of analysis are among the priorities.

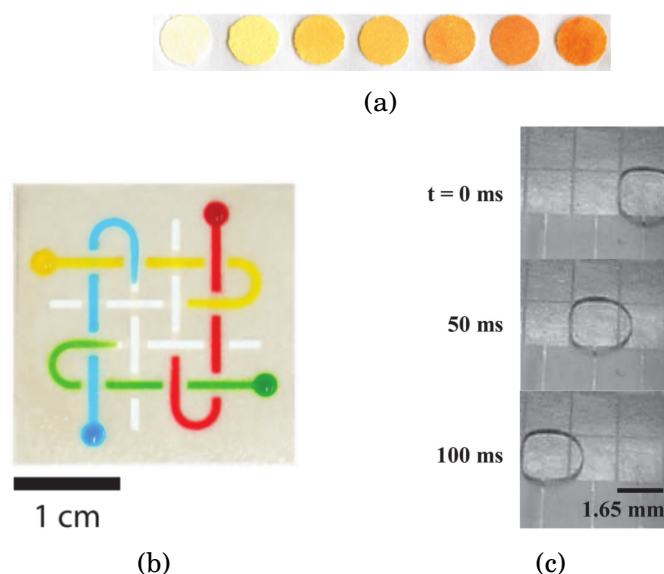


Figure 1: (a) Colourimetric detection of H_2O_2 on filter paper; increasing concentration from left to right (Ornatska et al., 2011). (b) Controlled fluid flow in three dimensions on a multilayered paper platform (Martinez et al., 2008a). (c) Manipulation of a droplet using an array of electrodes printed on paper (Fobel et al., 2014).

2.2 Cellulose and Nanocellulosic Materials

Cellulose and its derivatives are materials of great practical utility. They are used in, e.g., food additives (Commission Regulation, 2011, p. 13), building materials, clothing, and paper products. Major sources of cellulose have long been wood and cotton with cellulose content around 40–50 % and 90 %, respectively (Hon and Shiraishi, 2000, p. 98). The remainder of wood or cotton biomass consists mainly of lignin and hemicellulose, together with small amounts of extractives such as fatty acids and terpenes. Traditionally, cellulose fibres have been separated from their lignocellulosic matrix by mechanical, chemical, and thermal means (Smook, 1992, Ch. 4). The fibres can then be converted into their macro- and microfibril constituents, which are ultimately composed of cellulose molecules (cf. Figure 2). It has been proposed that the thinnest fibrils or elementary fibril of plant biomass consist of 36 cellulose chains (Ding and Himmel, 2006). Along a single fibril, their relative orientation varies from highly ordered, i.e. crystalline, regions to a more amorphous conformations. This hierarchical structure applies to fibres extracted from plants (Plackett, 2011) and also to fibres of bacterial origin (Mohite and Patil, 2014).

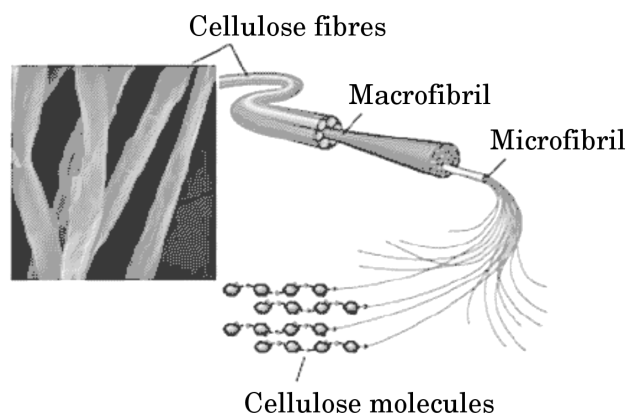


Figure 2: Hierarchical structure of a cellulose fibre. (Plackett, 2011, p. 153)

At the molecular level, cellulose consists of a linear chain of D-glucopyranose units bonded together by glycosidic β bonds at C^1 and C^4 of neighbouring glucose units (cf. Figure 3). The ends of a cellulose molecule are chemically different, as the end with C^1 -OH, i.e. the reducing end, is found in equilibrium with its aldehyde, while the end containing C^4 -OH, i.e. the non-reducing end, is not. Much of the chemical modification of cellulose takes advantage of its hydroxyl groups, which can undergo wide range of reactions typical for alcohols. (Klemm et al., 2005)

Another frontier of cellulose utilization takes advantage of aggregates of cellulose chains, i.e. nanofibrils or microfibrils, which are held together by hydrogen bonds and van der Waals forces between adjacent cellulose molecules. Materials composed of these nanosized fibrils are collectively addressed as nanocelluloses, which have by definition one of their fibril dimensions in the nanometer range. Nanocelluloses can be divided into three subcategories: bacterial nanocellulose (BNC), cellulose

nanocrystals (CNC), and CNF (Klemm et al., 2011). BNC is a product of biosynthesis of low-molecular weight sugars in certain bacteria. The nanofibrils form a fine network of highly crystalline nanofibrils with a high degree of polymerization. In CNC, most of the amorphous regions of nanofibrils have been dissolved with acid hydrolysis, which leaves relatively short and strong crystalline regions intact. Their physical dimensions are greatly influenced by the natural fibres from which they are isolated. In CNF, the fibrils are thicker and longer than those of CNC, and contain both amorphous and crystalline regions which together form high aspect-ratio nanofibrils. CNFs can be manufactured, e.g., through a high-pressure homogenization process coupled with enzymatic treatment, in which a cellulose suspension is fed multiple times through chambers connected with a thin channel where fibril bundles disintegrate due to shear forces (Pääkko et al., 2007). Nanofibrils can be further processed into self-standing films by pressure filtering a nanocellulose suspension through a mesh fabric followed by wet and hot pressing (Österberg et al., 2013b). Cellulose can also be spin coated onto silicon wafers by using its trimethylsilyl derivative, which allows the use of non-polar solvents such as toluene or chloroform. The resulting thin film is then hydrolysed back to cellulose with acid vapour (cf. Figure 5). (Kontturi et al., 2005)

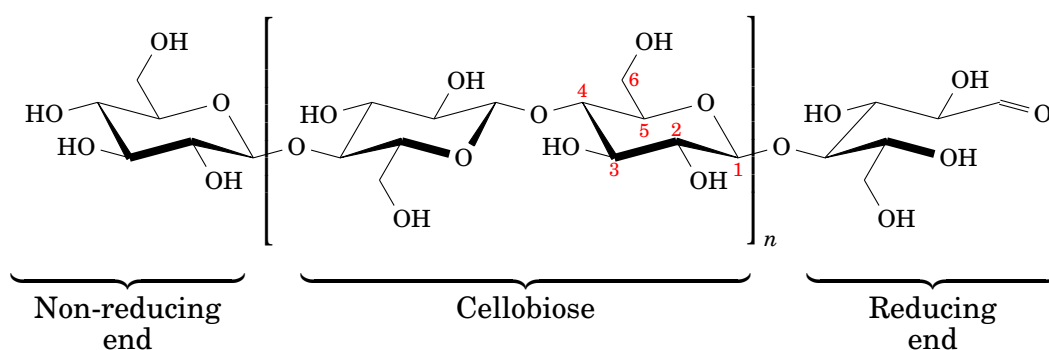


Figure 3: Structural formula for cellulose.

2.3 Silane SAMs

Nature exhibits a wide variety of phenomena akin to self-assembly. In general, these can be divided into processes where energy is not dissipated, e.g. crystal growth, and energy-dissipating processes, such as the life of a biological cell (Whitesides and Grzybowski, 2002). Self-assembly conveys a meaning that a more ordered state is achieved from a less ordered initial condition. One way to come about spontaneous assembly is to have asymmetric precursors, which are only partly inclined to interact strongly with each other. In silane SAMs, this is achieved through covalent head group-substrate interaction as explained shortly. The first studies towards understanding SAMs were done in 1946 when organic molecules were shown to form monolayers on solid surface with oleophobic and hydrophobic characteristics (Bigelow et al., 1946). It was also in the first half of the 20th century when the Langmuir-Blodgett method of monolayer film deposition was invented (Langmuir,

1920). Here the self-assembly takes place at the air-water interface, from where the film is transferred onto a substrate. Another popular monolayer format has long been thiols on gold surface (Ulman, 1996). More recently, self-assembly has become one of the defining paradigms of the bottom-up fabrication methodology in nanoscience (Zhang, 2003).

The structure of molecules constituting a SAM can be typically divided into three parts: an aliphatic or fluorinated tail, the head group, and the functional end group. The head group binds the molecule to the substrate via chemisorption, while the tail forms a network of van der Waals bonds with neighbouring monolayer molecules. Alkylsilanes fit into a generic chemical formula, $R_n\text{-Si-X}_{4-n}$, where R is a methyl-terminated hydrocarbon, while X is the leaving group (Arkles, 1977). Often, the leaving group is an alkoxy or chlorine. The attachment of silane molecules onto a cellulosic substrate is achieved via Si-O-C linkages between the silane head groups and the hydroxyl groups of cellulose.

A reason for SAMs multitude of uses arises from the versatility of the functional end group, which gives ways to engineer the surface energy and chemical functionality of the substrate. The chemistry of siloxane bonding has been utilized successfully for decades in sol-gel applications (Hench and West, 1990), and their use has subsequently matured and propagated to other disciplines. Illustrative examples where SAMs have emerged include: stiction prevention aids in microelectromechanical systems (Srinivasan et al., 1998), hydrophobic barriers in microfluidics (Nakashima and Yasuda, 2007), and use in selective electrodes of inorganic sensors (Turyan and Mandler, 1997). Additionally, due to their morphological and chemical uniformity, they are also utilized in fundamental research of surface phenomena, e.g. protein adsorption (Ostuni et al., 2001).

2.3.1 Growth Mechanism and Kinetics

A reaction pathway of siloxane monolayer formation onto cellulose is presented in Figure 4 (Arkles, 1977). In an ethanolic medium, the mechanism entails generally five reactions: (1) formation of ethoxysilane, (2) production of highly reactive silanols, (3) oligomerization of silanols, (4) physisorption of oligomers through hydrogen bonding on the surface, and (5) Si-O-C linkage formation with water condensation. Chlorosilanes can exhibit autocatalytic properties in ethanol as HCl is released by the initial alcoholysis. It can also contribute to the amount of water available for the subsequent hydrolysis, as HCl can react with ethanol forming water and chloroethane. In anhydrous conditions, alkoxy silanes can bond directly at the surface hydroxyls releasing alcohol (Arkles, 2006).

The amount of physisorbed water on the target surface and in the reaction medium determines partly whether a monolayer or multilayer growth takes place (McGovern et al., 1994). Oligomerization is also dependent on the number of leaving groups present in the silane, e.g. monochlorosilanes are unable to form such species altogether that could bond covalently onto the surface. The siloxane linkages between

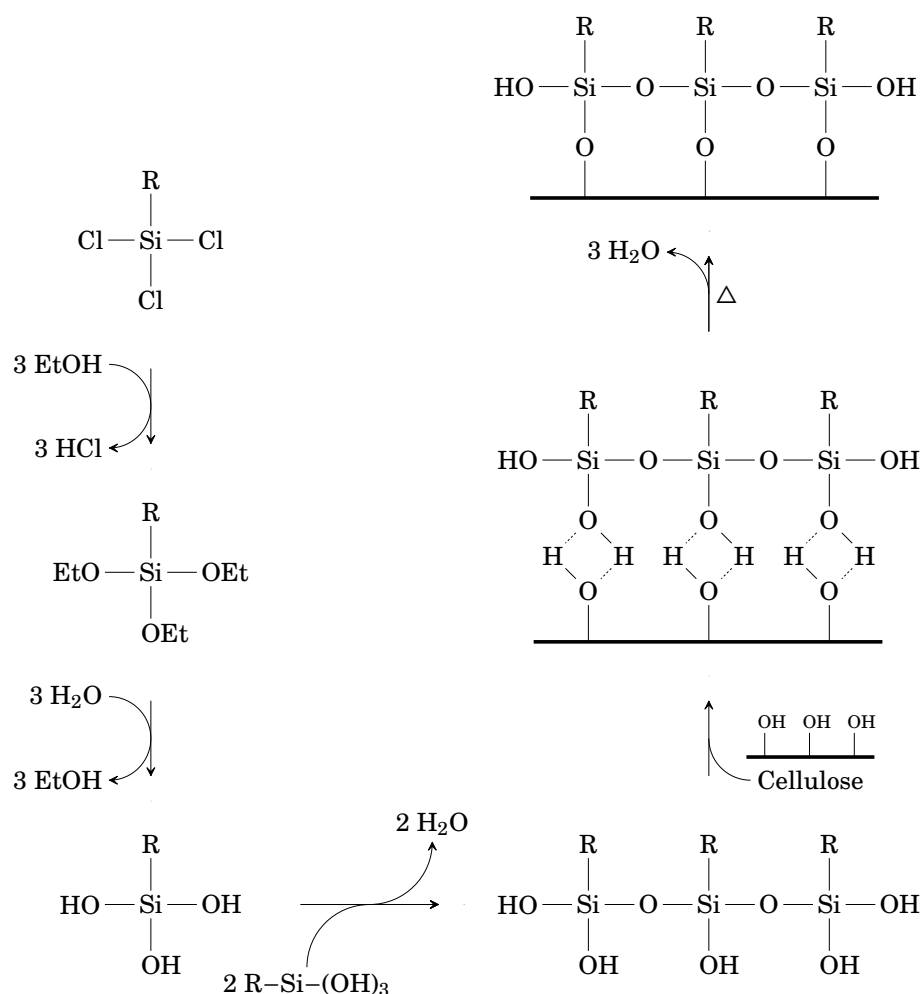


Figure 4: SAM growth mechanism from trichlorosilanes in ethanol. Trichlorosilanes reacts with ethanol to form triethoxysilanes and hydrochloric acid. The ethoxy groups are subsequently hydrolysed releasing ethanol. Oligomerization of silanes at the silanol moieties with water condensation, followed by hydrogen bonding onto the CNF film, and finally, water condensation as the Si–O–C linkage forms between the SAM and the substrate.

silanes with more leaving groups cannot extend throughout the monolayer with full coverage as siloxane bonding forces the hydrocarbon tails to tilt in opposite directions and thus sterically prevent further cross-linking (Stevens, 1999). Depending on the amount of leaving groups, the silanes have many configurations in which they can chemisorb onto the substrate, such as vertical polymerization (Fadeev and McCarthy, 2000), and for this reason, monochlorosilanes are considered less disruptive in terms of surface morphology.

Compared to monolayers grown in liquid phase, vapour phase growth is generally favoured when high-quality monolayers are desired, as the polymerized silane species are less likely to vaporize due to their lower vapour pressure (Sugimura et al., 2002), while they can readily deposit in liquid medium with excessive water

content (Brandriss and Margel, 1993). A great body of work with silane monolayers is done on silica surfaces, which bear a similar hydroxyl-terminated functionalities as cellulose. Experiments show that the formation of silanols takes place at the physisorbed water layer on the surface in vapour phase growth (Tripp and Hair, 1995).

The growth rate of SAMs is usually approximated with the Langmuir adsorption kinetics (Schreiber, 2000). This model assumes negligible desorption and a growth rate that is limited by the available surface reactive sites. In this framework, the change in surface coverage (Θ) with respect to time (t) can be stated as

$$\frac{d\Theta}{dt} = k(1 - \Theta), \quad (1)$$

where k is the rate constant. Integrating this expression gives

$$\Theta = 1 - \exp(-kt). \quad (2)$$

The Langmuir kinetics thus predicts a large initial growth rate, which slows down as the surface bears fewer reactive groups, though kinetic studies indicate a deviation from the predicted coverage of Langmuir kinetics during the initial adsorption (Richter et al., 2000). Whether silanes form large islands on the surface followed by a slower filling of the remaining free surface, or follow a more uniform growth mode is highly dependent on the medium in which the growth proceeds (Schreiber, 2000).

2.3.2 Degradation

Acidic and alkaline conditions have a catalytic effect on hydrolysis, which is commonly used in e.g. conversion of trimethylsilylcellulose to cellulose (see Figure 5) (Buchholz et al., 1996). This also motivates the study on stability of SAMs in vapours of HCl and NH₃ in addition to their long-term stability in humid atmosphere, as the bonding is identical to trimethylsilyl groups, with the difference of a larger hydrophobic alkyl chain. The kinetics of hydrolysis-driven degradation originates likely from structural imperfections in the monolayer, allowing water penetration into the SAM-cellulose interface, leading to hydrolysis of Si–O–C or displacement of uncondensed silanols from the surface with water (Pellerite et al., 2002).

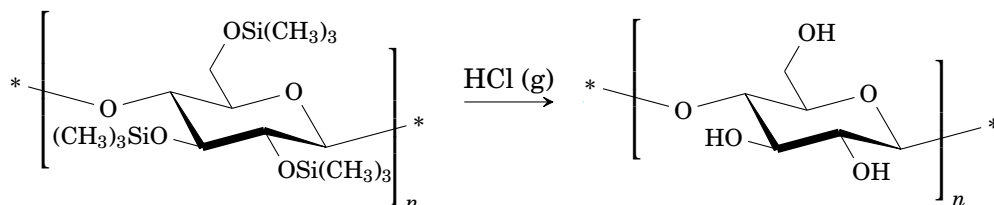
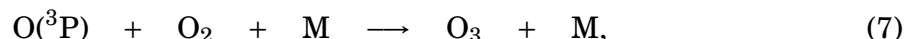
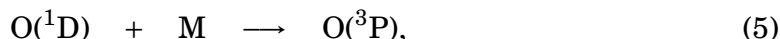
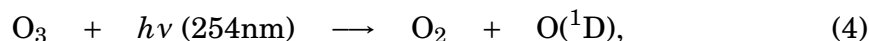
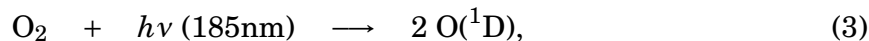


Figure 5: Regeneration of trimethylsilylcellulose to cellulose with acid vapour.

Photochemical methods can be used to remove alkyl chains of silane monolayers, for example, deep UV light (193 nm) (Dulcey et al., 1991) and vacuum UV light (172 nm) (Sugimura et al., 2000) has been used to cleave Si–C and C–C bonds in vacuum. Sub-200 nm wavelength photons can initiate the formation of atomic oxygen, hydroxyl radicals (HO[•]), and ozone in air according to:



where M is an inert molecule (DeMore et al., 1997). Ye et al. (2005) proposed a mechanism for alkyl chain degradation under UV light and ozone exposure, which starts with hydrogen abstraction at the terminal carbon, producing peroxide radicals after oxidation. This can react further with UV light or HO[•], forming alkoxy radicals, which produce aldehydes after reacting with O₂. C–C cleavage occurs when the aldehyde groups react with UV light or oxygen (cf. Figure 6). In addition to aldehydes, the surface bears other functional groups after UV/O₃ exposure, such as hydroxyls and carboxyls, which leave the film in an increasingly hydrophilic state as the film degradation proceeds. Ye et al. (2005) further observed that ground state atomic oxygen, O(³P), is the dominant oxidant for 184 nm and longer wavelengths. The initial hydrogen abstraction and the final cleavage of C–C might be mediated mainly by species with large mean free path, which hinders its use for patterning purposes unless the direct photolysis route can be made prevailing.

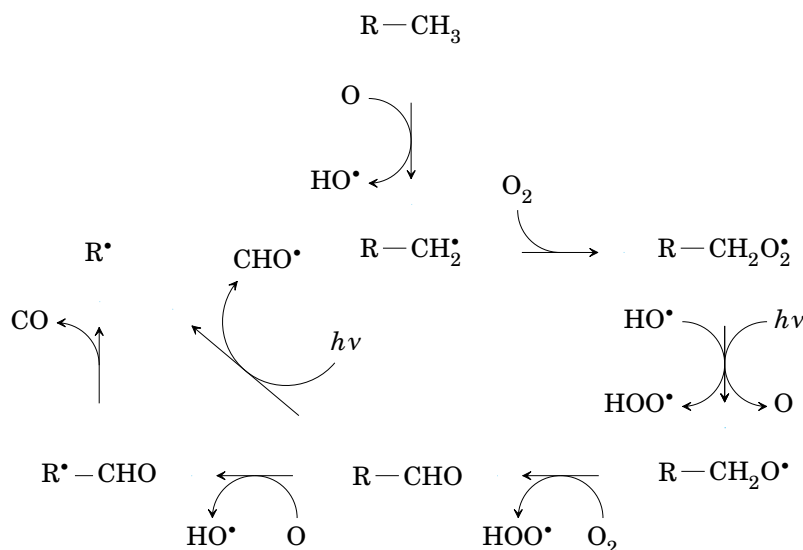


Figure 6: Photodissociation mechanism of C–C at the alkyl chain of silane SAMs as proposed by Ye et al. (2005).

The thermal stability of SAMs is less of a concern for silanes grown onto cellulosic substrates as cellulose starts to degrade at similar temperature ranges as silanes,

experiencing e.g. depolymerization, oxidation, and dehydration below 300 °C (Simoneit, 2002). Silane SAMs grown on silicon have been reported to be stable up to around 150–200 °C in air (Srinivasan et al., 1998; Zhuang et al., 2006), while sustaining integrity up to 250–450 °C in N₂ atmosphere and vacuum (Chandekar et al., 2010; Kluth et al., 1997). Generally, the temperature region where irreversible changes occur varies greatly according to the end group composition and packing density of silanes (Chandekar et al., 2010).

2.4 Wetting and Wicking

The importance of surface tension is prominent when handling small volumes of liquids due to a large liquid-vapour interface relative to the fluid volume. The molecular basis of surface tension arises from the energetically higher potential of molecules at the vapour-liquid interface relative to the bulk of the liquid where water molecules are surrounded by other water molecules to which they can form temporary hydrogen and van der Waals bonds, whereas molecules at the vapour-liquid interface can do so only partially. This leads to an energy difference as more energy is invested in the bonds on average in the bulk relative to the surface. An outcome of surface tension is that if a liquid surface exhibits curvature, then there must exist a pressure difference across it, as the liquid-vapour interface affects the mechanical equilibrium of the liquid-vapour system. (Butt et al., 2003, Ch. 2) The explicit relation between the pressure difference (Δp), the surface tension (γ), and the curvature is known as the Young-Laplace equation:

$$\Delta p = \gamma \left(\frac{1}{R_1} + \frac{1}{R_2} \right), \quad (8)$$

where R_1 and R_2 are the principal radii of curvature of the liquid-vapour interface. Equation 8 can be derived, e.g., from variational principles (Landau and Lifshitz, 1987, pp. 230–231) or by using the grand canonical scheme (Reichl, 2009, pp. 142–143).

When a liquid droplet is placed on a solid surface, it attains a shape corresponding to the minimum of the Gibbs free energy (G). Its contact angle (θ) is related to the three interfacial free energies (γ) acting in the system (see Figure 7). The shape of the droplet and its three-phase line do not necessarily correspond the global minimum of G , leading to a range of possible contact angles (Marmur, 2006). The effect of multiple metastable three-phase line configurations can be observed when water is withdrawn and added to a droplet, producing the receding and advancing contact angles, respectively. The difference of these two angles is called the contact angle hysteresis. (Gao and McCarthy, 2006)

Two surface modifications can be made when engineering the wetting behaviour of a solid surface, namely, changing the surface roughness or changing the palette of surface chemical groups. The effects of these modifications can be approximated with Young, Wenzel, and Cassie-Baxter models introduced next (see Figure 8). The

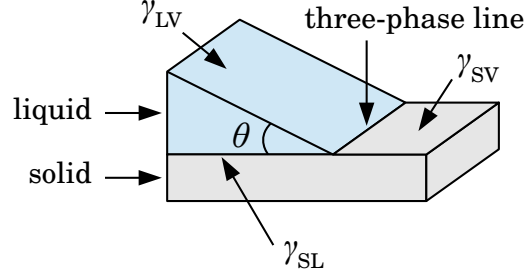


Figure 7: Liquid-vapour (LV), solid-vapour (SV), and solid-liquid (SL) interfacial free energies (γ) and contact angle (θ) of a droplet on a solid surface. (Butt et al., 2003, p. 119)

minimization of Gibbs free energy can be used as the starting point when deriving the aforementioned models (Whyman et al., 2008). For an ideally flat and chemically homogeneous surface, the relation between the different interfacial free energies and the contact angle is given by the Young's equation:

$$\cos \theta_Y = \frac{\gamma_{SV} - \gamma_{SL}}{\gamma_{LV}}, \quad (9)$$

where γ_{SV} , γ_{SL} , and γ_{LV} are the solid-vapour, solid-liquid, and liquid-vapour interfacial free energies, respectively (Young, 1805). The effect of surface roughness can be included by adding a roughness factor (r), which denotes the fraction of the true surface area to projected surface area. With this inclusion, the apparent contact angle is given by the Wenzel equation (Wenzel, 1936):

$$\cos \theta_W = \frac{r(\gamma_{SV} - \gamma_{SL})}{\gamma_{LV}}. \quad (10)$$

According to Equation 10, an increase in surface roughness translates into an increase in apparent contact angle when $\theta_Y > 90^\circ$ and to a decrease for $\theta_Y < 90^\circ$. In the Cassie-Baxter model (Cassie and Baxter, 1944), the heterogeneity of the surface chemistry, of N variety, is included by adding in the fractions (Φ_i) of their respective surface coverage:

$$\cos \theta_{CB} = \frac{1}{\gamma_{LV}} \sum_{i=1}^N \Phi_i (\gamma_{i,SV} - \gamma_{i,SL}), \quad (11)$$

where $\sum_{i=1}^N \Phi_i = 1$.

Although the surface chemistry in Cassie-Baxter model and the roughness in Wenzel model are heterogeneities introduced to an ideal surface, they are still accounted for in a homogeneously distributed fashion. When considering more realistic systems, the above models are inadequate as they rely on the interfacial free energies while ignoring the behaviour of the three-phase line (Gao and McCarthy, 2007). For instance, two binary composite surfaces with identical roughness factors can exhibit different contact angles depending on the conformation of the three-phase line (see Figure 9) (Youngblood and McCarthy, 1999). Hence, more complex models have been devised that give the above results as a special case. For example, the

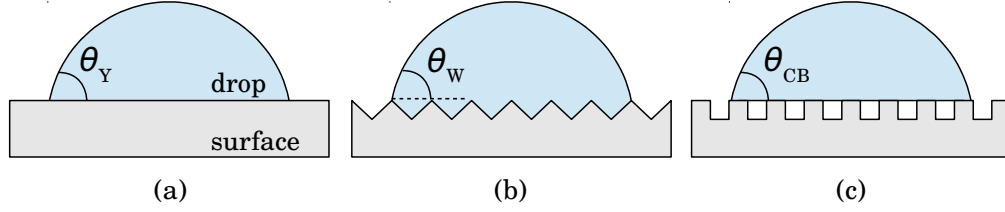


Figure 8: Illustration of the different wetting models with their apparent contact angles: (a) Young, (b) Wenzel, and (c) Cassie-Baxter ($N = 2$). (Whyman et al., 2008)

contact angle of a droplet on a chemically heterogeneous rough surface with the inclusion of line tension (λ) at the three-phase line ($\partial\Gamma$, parametrized with s) can be stated as

$$\cos\theta_{\text{eff}} = \sum_i l_i(\gamma_{i,\text{SV}} - \gamma_{i,\text{SL}}) - \frac{\oint_{\partial\Gamma} ds \nabla \cdot \lambda(s) \hat{\mathbf{n}}(s)}{\oint_{\partial\Gamma} ds}, \quad (12)$$

where θ_{eff} is the average contact angle around the drop, l_i are the portions of the total $\partial\Gamma$ of material i , and $\hat{\mathbf{n}}$ is a unit normal vector to $\partial\Gamma$ (Swain and Lipowsky, 1998). The values of $\lambda(s)$ and $\partial\Gamma$ are determined experimentally. Equation 12 is a more local model due to the line integral term, which vanishes when the line tension is negligible.

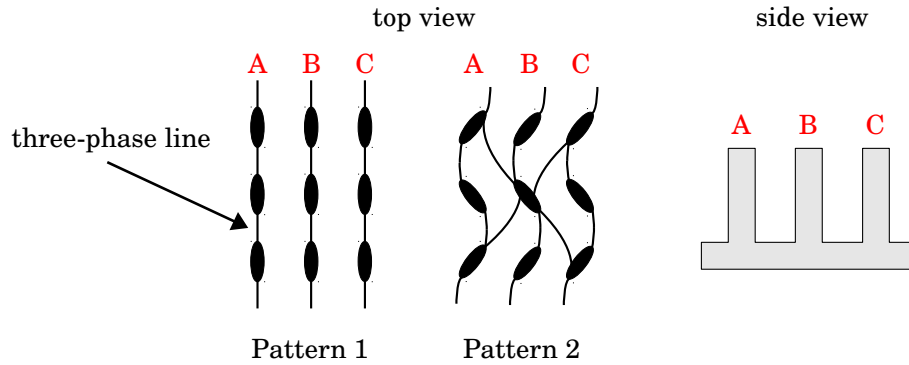


Figure 9: An example how the shape of a three-phase line can be tied to the morphology of the substrate while keeping the roughness factor constant. In Pattern 1, the three-phase line is pinned due to high energetic cost of transitions $A \leftrightarrow B \leftrightarrow C$. This can be seen as a larger contact angle hysteresis compared to Pattern 2 which allows multiple three-phase line configurations and a smoother transition between A and C. (Youngblood and McCarthy, 1999)

Wetting of porous solids differs from the above treatment in that one has to consider also the effect of wicking, i.e. intake of fluid into the porous network, which originates from the capillary action generated by the pores. The volumetric flow rate (Q) in such a material is stated by the Darcy's law:

$$Q = -\frac{\kappa A}{\mu L} \Delta p, \quad (13)$$

where κ is the hydraulic conductivity of the substrate, A is the area of the pore cross-section, μ is the dynamic viscosity of the fluid, and L is the length of the channel (Bear, 1988, p. 120). The flow rate can be thus varied by changing the channel length, and therefore, Equation 13 can be used to predict reagent movement in lateral flow strips (Osborn et al., 2010). Modelling of wicking can be further improved by taking into account pore size changes due to swelling of the fibrils, for example, Masoodi and Pillai (2010) proposed a model in good agreement with experimental results when the increase in volume of fibrils due to swelling is equal to the volumetric intake of the adsorbate liquid.

2.5 Protein and Polyelectrolyte Adsorption

A comprehensive explanation of protein adsorption onto surfaces bearing different chemical groups is still missing, but Chapman et al. (2000) observed that characteristics of a surface that inhibits protein adsorption include: polar functional groups, neutral surface charge, absence of hydrogen-bond donors, and presence of hydrogen-bond acceptors. Multiple interactions ultimately define the adsorption behaviour of a protein, but a general notion is that the adsorption should be energetically favourable, i.e. leading to a smaller Gibbs free energy, or

$$\Delta G = \Delta H - T\Delta S < 0, \quad (14)$$

where H is enthalpy, which includes changes in energy, T is the temperature, and S is the entropy, which accounts changes in conformation, e.g. loss of degrees of freedom (Déjardin, 2006, p. 119).

Certain considerations can be made from the amphipathic nature of proteins, which affects their conformation in an aqueous environment as the hydrophilic components are predisposed to align themselves towards water molecules while the hydrophobic components are buried within them. In hydrophobic interaction, the buried hydrophobic components interact with a non-wetting surface, or with another hydrophobe, via an energetically favoured change in conformation that exposes the two components to each other and thus reducing the disruption of water hydrogen bonding network (Chandler, 2005). The extent to which a protein can change its conformation is limited by the strength of its intramolecular interactions and bonds. Additionally, adsorption can be affected by the ease at which the surface dehydrates upon interacting with the adsorbate, which in hydrophilic surfaces could act against adsorption (Norde and Zoungrana, 1998). Similarly inhibiting aspects may arise from ionic species of the solvent that can compete with adsorption of proteins (Wei et al., 2009).

The pH of the solution can affect the adsorption properties of proteins by changing the nature of the electrostatic interaction between its segments, other proteins, and surfaces as the amino acid constituents of a protein can bear a charge in aqueous solutions due to different ionization states. At a certain pH, the amino acids of a protein will not carry a net charge due to equal number of anionic and cationic

groups. This is termed the isoelectric point (pI). Below pI the protein has a positive charge and negative above it, and in this manner, the electrostatic interactions can change at different pH. (Stryer, 1995, pp. 18–19, 48)

Polyelectrolyte adsorption onto solid surfaces is affected e.g. by surface charge, polyelectrolyte charge, salt concentration, and solubility of the polymer in the solvent. Additionally, the size of the polyelectrolyte can affect the adsorption onto porous surfaces such as cellulose fibres, as small polymers can diffuse more easily into the pores after the initial adsorption (Wågberg, 2000). The salt concentration of the solvent can increase or decrease the adsorption depending on the relative strengths of electrostatic and non-electrostatic interactions (van de Steeg et al., 1992). When electrostatic forces dominate, high salt concentration decreases adsorption due to screening, i.e. affecting the Debye length of charged surfaces. However, if non-electrostatic interactions are dominant, increasing salt concentration can have an opposite effect as uncharged polymers can change conformation to accommodate themselves on the surface. Screening of charges by ions can also affect protein adsorption (Zhang et al., 2007).

3 Experimental

An account of the materials used in this thesis is given next, after which the experimental methods are explained. This section ends with the description of the characterization methods and their governing principles.

3.1 Materials

This section lists the chemicals and materials used in this thesis.

3.1.1 Chemicals

n-Octyldimethylchlorosilane (S1) (> 95 %), *n*-octylmethyldichlorosilane (S2) (> 95 %), *n*-octyltrichlorosilane (S3) (> 95 %), and 1,2-bis(trichlorosilyl)decane (S6) (> 95 %) (see Figure 10) were purchased from Gelest, Inc. (USA). NaCl ($\geq 99.9\%$), analytical grade acetone and toluene were acquired from VWR Chemicals (Belgium). KCl ($\geq 99.5\%$) and KH_2PO_4 ($\geq 99.5\%$) were obtained from Merck KGaA (Germany), while BSA lyophilized powder ($\geq 98\%$) and anhydrous Na_2HPO_4 ($\geq 99.0\%$) were purchased from Sigma-Aldrich Chemie (Germany). PEI (30 % aqueous solution, MW: 50 000–100 000) was acquired from Polysciences, Inc. (Pennsylvania, USA). Ethanol ($\geq 99.7\%$) was purchased from Altia Oyj (Finland). All chemicals were used as received.

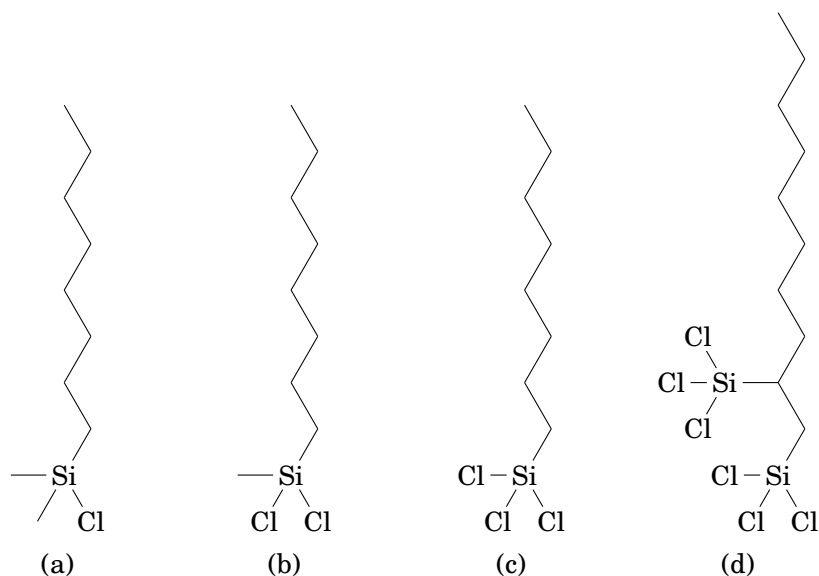


Figure 10: The silanes used in this thesis: (a) S1, (b) S2, (c) S3, and (d) S6.

3.1.2 CNF Film

A roll of CNF film was obtained from VTT Technical Research Centre of Finland (Espoo). The film was stored in constant 50 % RH at room temperature.

3.2 Methods

In this section, the growth methods of the silane SAMs are described in addition to the various stability tests to which the silane-modified films were subjected to. The experimental description of BSA and PEI adsorption is given subsequently, after which the principles of contact angle measurement, atomic force microscopy, and X-ray photoelectron spectroscopy are explained.

3.2.1 UV Ozonation

CNF film surface activation and stability under UV/O₃ was accomplished with UV Ozone ProCleaner™ (BioForce Nanosciences, Inc., USA). The primary wavelength of the UV light is 254 nm and a secondary wavelength of 185 nm, which together initiate the generation of atomic oxygen and ozone (see Section 2.3.2). The combined effect of UV light and reactive oxygen species leads to a cleaner and more hydrophilic film surface due to decomposition and evaporation of small hydrophobic organic contaminants and thus also increasing the availability of surface hydroxyl groups, in addition to generating more polar functional groups due to oxidation. (Österberg et al., 2013a)

3.2.2 SAM Growth Methods

The CNF film was removed from storage at least 24 h before use. The SAM growth was carried out by either immersing the film into a silane solution or by exposing the film to silane vapour. In both cases, the films were activated in UV ozonator for 10 min before the silane treatment. In the liquid phase modification, 20 mL of toluene-silane solution was prepared for ca. 8 cm² piece of CNF. In the vapour phase growth, an 8 cm² CNF film piece was placed in a desiccator along with a ca. 2 mL of silane, after which the desiccator was evacuated to a low pressure. Regardless of the reaction medium, after the reaction was terminated, the films were rinsed with ca. 15 mL of toluene and allowed to dry in a fume hood until the excess toluene had seemingly evaporated. The films were then stored between two blotting papers inside a vacuum desiccator until further use.

3.2.3 Stability Tests

The test in ambient environment was carried out at ambient laboratory conditions. The sample was placed between two blotting papers inside a Petri dish covered from light for 1–8 weeks, while the lowest and highest temperatures and RH values were recorded continuously during the experiments. The measurements concluded that temperature varied between 19.7 and 26.9 °C, while RH varied between 21 and 51 %. The 50 % RH test took place in the same space which was used to store the CNF film roll. The samples were exposed to the air directly for 1–4 weeks. In the 100 % RH test, the films were placed in a desiccator along with Milli-Q water. The desiccator was then evacuated to the vapour pressure of water and left for 1–4 weeks. HCl and NH₃ vapour experiments were similar to the 100 % RH test, only that 10 vol-% HCl or NH₃ was used in the vacuum desiccator instead of Milli-Q water. Also, the experiments lasted only 1 h. The stability of samples under UV light was tested with 254 nm and 366 nm wavelength light for 1 h from 1 cm distance. The irradiance of the 366 nm lamp was measured to be ca. 3 mW/cm² at that distance. After all of the above experiments, excluding the ambient test, the films were rinsed with ca. 15 mL of toluene and allowed to dry, after which the samples were stored overnight in a vacuum desiccator before characterization.

3.2.4 BSA and PEI Adsorption

The adsorption of BSA (0.1 wt-%) and PEI (1 wt-%) was studied in Milli-Q water adjusted to pH 4 with acetic acid (AA) and phosphate buffered saline (PBS) adjusted to pH 7 with HCl. PBS had a concentration of 10 mM, i.e. containing 8.0 g/L of NaCl, 0.2 g/L of KCl, 1.44 g/L of Na₂HPO₄, and 0.24 g/L of KH₂PO₄. Four types of films were used, namely native CNF film, native CNF film UV/O₃-activated for 10 min, S1-modified CNF film, and S1-modified CNF film subjected to UV/O₃ for 30 min.

Adsorption was carried out as follows. 30 mL of BSA or PEI solution was poured over a ca. 3 cm² piece of film and left for 30 min, after which about 2/3 of the solution was removed and the rest was diluted to ca. 1:5 with the buffer solution. The dilution was repeated three times with the buffer and two times with deionized water. The film was then removed from the solution and immersed into Milli-Q water before allowing it to dry in ambient laboratory conditions. The presence of BSA or PEI was monitored by tracking the relative atomic percentage of nitrogen determined from XPS survey spectra.

3.2.5 Contact Angle Measurement

Static WCA measurements were carried out with CAM 200 (KSV Instruments Ltd., Finland), which has a computer-controlled water dispensing system and a droplet shape analysis software. The contact angle measurement is based on the shape of a

sessile droplet by fitting a curve at its air-water interface. The measurement setup is depicted schematically in Figure 11. At least three measurements were made for each sample using Milli-Q water droplets. The results were averaged to give the mean WCA, while a 95 % confidence interval (CI) was used to represent error bounds for the mean.

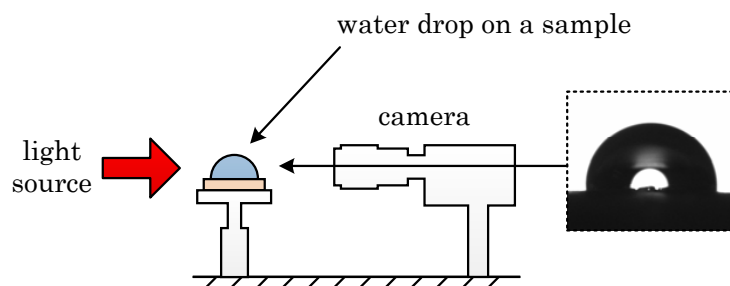


Figure 11: Schematic illustration of the principle of contact angle measurement. A solid sample is irradiated from one side with monochromatic light as a droplet is placed on the sample. A camera captures images of the meniscus from the opposite side. Computer software fits a mathematical expression on the liquid-vapour interface and calculates the contact angle.

3.2.6 Atomic Force Microscopy

AFM is used to probe the surface morphology of solid samples with sub-nanometer vertical resolution. Generally, it can be operated in three modes: non-contact mode, tapping mode, and contact mode. For soft samples, e.g. many polymers and ligno-cellulosic materials, the tapping mode is the prevailing characterization mode as it allows minimal contact with the sample. In tapping mode, the cantilever of AFM is oscillated close to its flexural resonance frequency near the surface of the sample. The attractive and repulsive forces exerted by the surface atoms on the cantilever tip cause it to change its vibrational amplitude as it pans across the surface. This signals the piezoelectric actuator to increase the sample-cantilever distance, if the amplitude decreases, and to decrease the distance when the amplitude increases. A topographical map of the surface can be formed by measuring the amount of vertical movement needed to keep the cantilever's amplitude constant while moving it across the surface (cf. Figure 12). (Haugstad, 2012, Ch. 1.4)

At least three $10 \times 10 \mu\text{m}^2$ images with 512 scan lines were acquired per sample with MultiMode™ Scanning Probe Microscope (Digital Instruments, Inc., USA). The images were post-processed with a third degree flattening, which centers the height data and removes tilt and bow. The imaging was carried out in the tapping mode in ambient air with silicon cantilevers purchased from Bruker Corporation (USA).

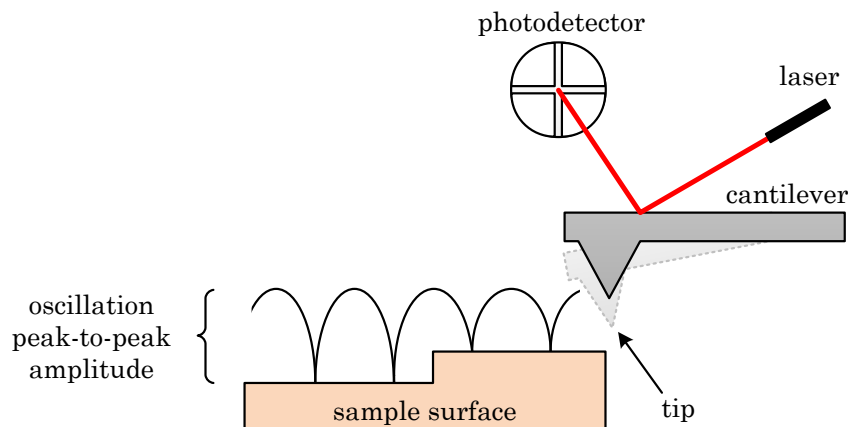


Figure 12: Schematic illustration of the principle of AFM. As the amplitude of the cantilever oscillation changes due to surface topography, the cantilever-sample distance is changed such that the original amplitude is regained, allowing a topographical image to be composed from the distance adjustments.

3.2.7 X-Ray Photoelectron Spectroscopy

In XPS, a solid sample is irradiated with monochromatic photons with energy (E_P) in the X-ray region of the electromagnetic spectrum, where the photon energy is favourable for interaction with core electrons of the sample, causing a detectable emission of the core electron (also photoelectron). Although photoelectrons are emitted throughout the sample, only the top few nanometers contribute significantly to the spectrum, as the electrons emitted in the bulk are likely to lose energy through inelastic scattering and thus fail to reach the ultra-high vacuum. The kinetic energy of the photoelectron (E_{KE}) can be used to deduce the corresponding element from the relation to its binding energy (E_{BE}), which is given by the energy conservation equation of elastic scattering:

$$E_{BE} = E_P - E_{KE} - \phi, \quad (15)$$

where ϕ is the work function of the detector (see Figure 13) (van der Heide, 2012, p. 9). The spectrum can then be constructed by counting the detected electrons, in counts per second (CPS), as a function of binding energy. The chemical environment of the element is seen as a shift in the spectral peak's fine structure. This is due to deviations in the interaction of the valence electrons with neighbouring bonding atoms, thereby quantitatively affecting the attractiveness between the core electrons and the nucleus. This altered attractive interaction shifts the binding energy above or below the value corresponding to unbonded atom depending on whether the bonding interaction results in loss or gain in electron density of the valence shell of the atom under consideration. (van der Heide, 2012)

The XPS spectra were obtained with Kratos AXIS ULTRA electron spectrometer used in conjunction with a mono Al- $K\alpha$ source (100 W) and a charge neutralizer.

The assignment of spectral peaks was done as follows: Si 2p at 102 eV, Si 2s at 153 eV, C 1s at 285 eV, N 1s at 397 eV, and O 1s at 529 eV. C 1s high-resolution spectra were recorded with a pass energy of 20 eV, from which the deconvoluted peaks were assigned to C–C at 285.0 eV, C–O at 286.7 eV, C=O at 288.2 eV, and O–C=O at 289.5 eV. 95 % CI was used to represent error bounds for the relative atomic percentages determined from the spectra.

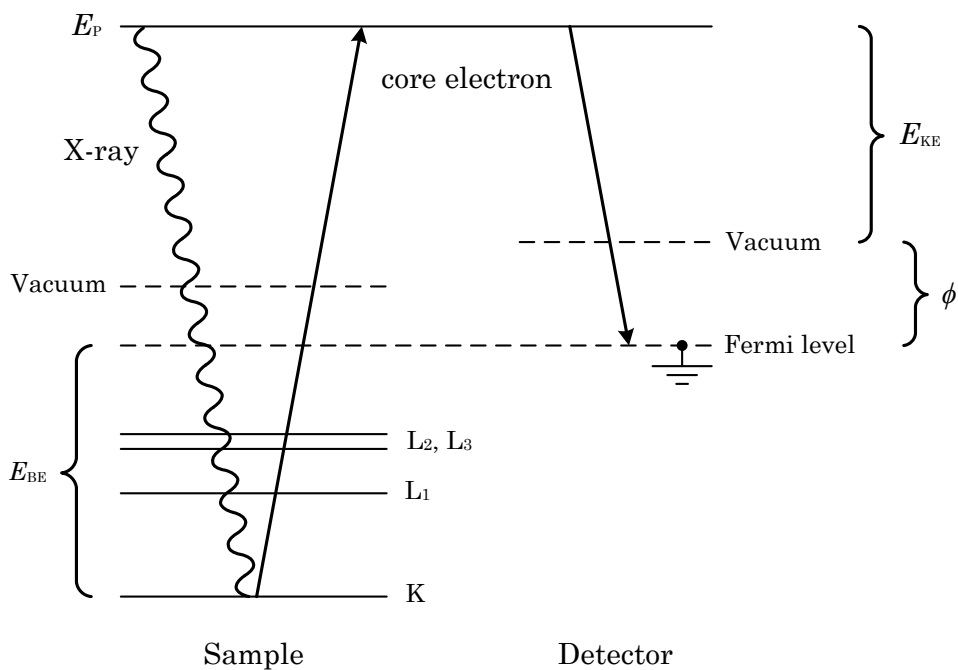


Figure 13: A schematic illustration of Equation 15, where E_P is the photon energy, E_{BE} is the core electron binding energy, E_{KE} is the electron kinetic energy at the detector, ϕ is the detector work function, while K , L_1 , L_2 , and L_3 are atomic orbitals (van der Heide, 2012, p. 67).

4 Results and Discussion

This section presents the results of this thesis. The characterization of the native CNF film is covered first, after which the results of SAM growth kinetics are presented, followed by the results of stability tests. BSA and PEI adsorption are covered thereafter.

4.1 CNF Film Characterization

The native CNF film had a WCA of $21.7^\circ \pm 2.1^\circ$ after 24 h from removing the film from its storage. After a 10 min UV/O₃ activation, the WCA decreased to $14.9^\circ \pm 3.6^\circ$ with no apparent effect on the surface morphology of the film (Figure 14c). Fibrils ca. 1 μm wide can be seen in the AFM images shown in Figure 14, but predominantly their widths were below 100 nm. Additionally, the film surface was covered partly in granular features (Figure 14b), which were assumed to be additives included during the making of the film. This affects the type of conclusions that can be made of morphological changes as the film is quite heterogeneous in this respect.

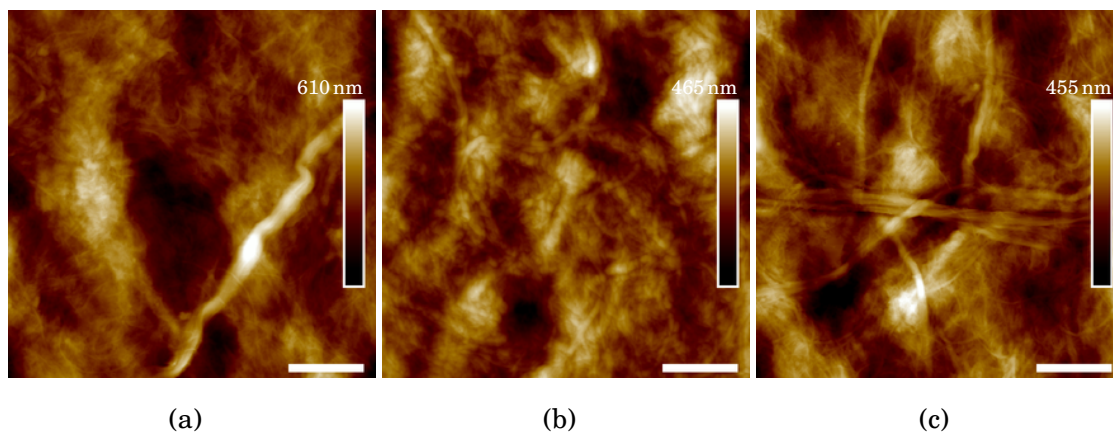


Figure 14: AFM height images taken from (a), (b) native CNF film and (c) CNF film UV/O₃-activated for 10 min. The scale bar represents 2 μm .

The survey and high-resolution C 1s spectra acquired with XPS are presented in Figure 15. The survey spectrum shows the presence of oxygen and carbon (Figure 15a) with O/C ≈ 0.58 , compared to 0.83 of pure cellulose. The so-called cellulose fingerprint region is visible in the high-resolution C 1s (Figure 15b). It appears slightly distorted: a roughly 3:1 ratio of C–O to C=O originating respectively from the carbon atoms that are bonded to oxygen with single bonds and from carbon singly bonded to two oxygen atoms (cf. Figure 3). Also visible are small C–C and O–C=O components, likely from carbonaceous contamination or lignocellulosic residues and carboxyl groups, respectively (Johansson, 2002). The presence of contamination is clearly diminished by the UV/O₃ activation (Figure 15b).

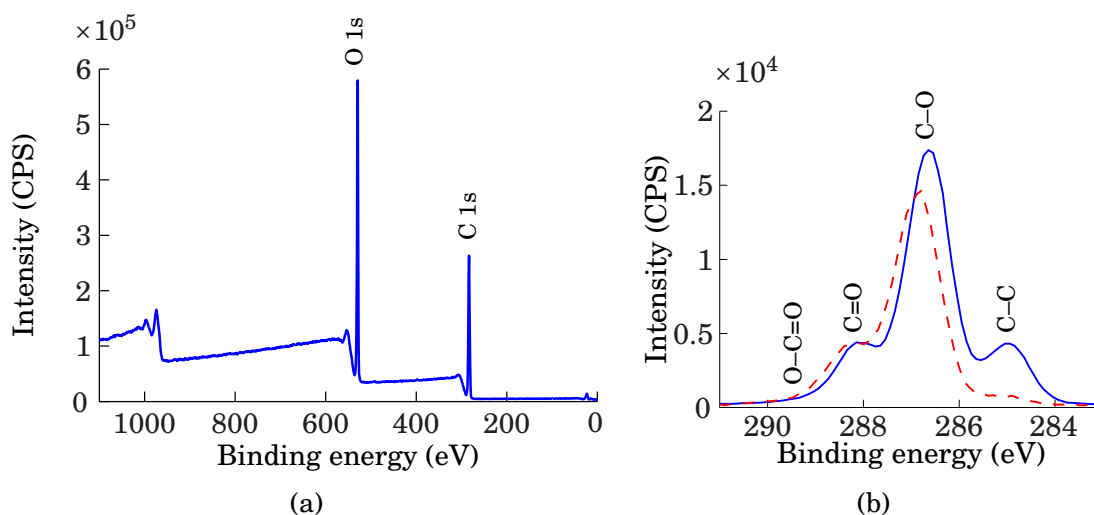


Figure 15: (a) Native CNF XPS survey spectrum and (b) high-resolution C 1s of native CNF film (—) and CNF film UV/O₃-activated for 10 min (- - -).

4.2 Growth Kinetics

Of the solvents experimented with in the silane modification, toluene produced the best results. This remark was followed by a more comprehensive kinetic study, the results of which are shown in Figure 16. S1 and S2 show a clear increase in WCA with 10 mM and 100 mM concentrations and the data suggests that the surface is fully saturated after 17 h. S3 and S6 produce a marked increase at much lower concentrations, i.e. below 1 mM, and seem to be much faster in expending the available surface reactive sites. AFM imaging revealed no apparent changes in surface morphology after S1 and S2 treatments (Figures 18b and 18c), but after S3-modification, the fibrils seem to be more pronounced or swollen (Figure 18d), which might be linked to a multilayer growth mode. The effect of silane-modification appears in the XPS spectra as Si 2s and 2p peaks and also in the high-resolution C 1s as an increase in the C–C component, originating mostly from the silane alkyl chains, and as a decrease in C–O as cellulose attains the silane SAM. A complete data set of the different atomic percentages and C 1s components is presented in Figure 19, which show a similar trend for S1, S2, and S3.

During the growth of S6, cross-linked silane lumps have likely deposited on the film surface (Figure 18e). Attaining a lump-free S6-modification was not achieved and for this reason S6 was excluded from the stability tests and further characterization with XPS. Regardless, S6 growth kinetics was investigated in vapour phase, but similarly high WCAs were not achieved as the WCA seems to reach its maximum at ca. 95° (Figure 17). AFM imaging showed no cross-linked lumps on the film treated for 17 h with S6 vapour (Figure 18f). For the longest treatment time of 48 h, the silane had cured somewhat during the last 24 h, which might have had an effect on the silane vapour pressure inside the desiccator.

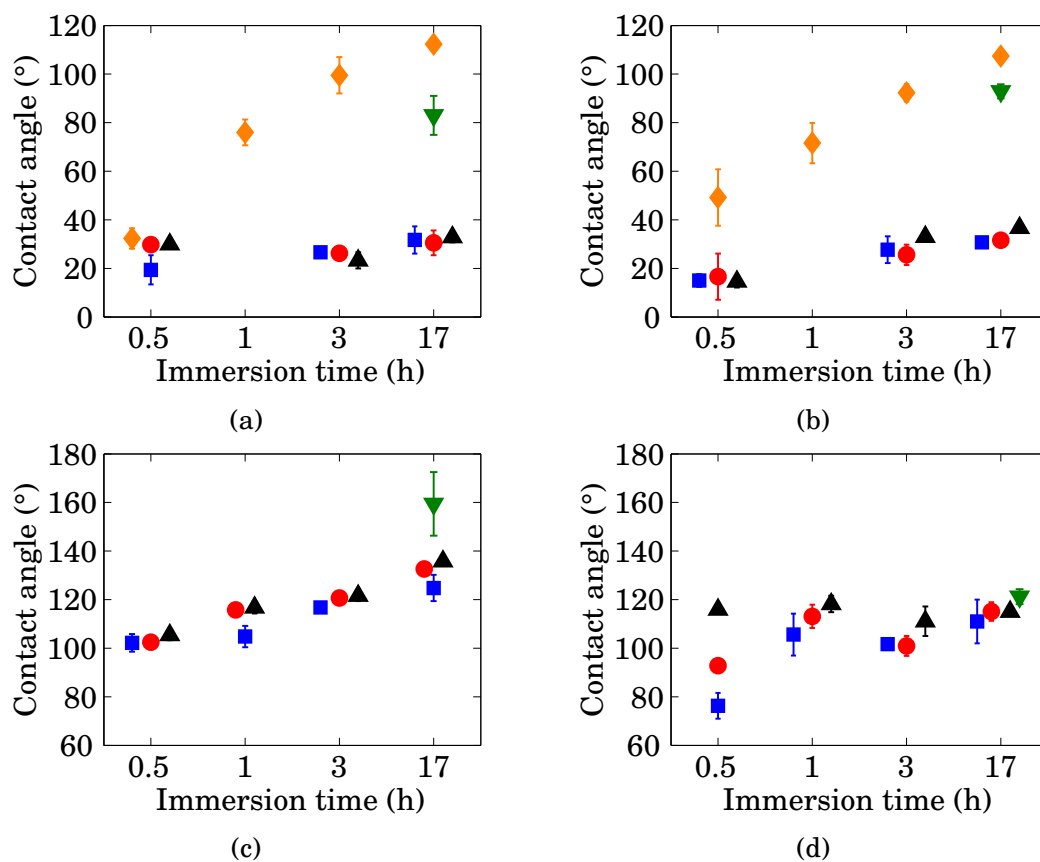


Figure 16: Water contact angle ($\pm 95\%$ CI) of CNF films modified with (a) S1, (b) S2, (c) S3, and (d) S6 in liquid phase as a function of immersion time. Silane concentration: ■ 0.1 mM, ● 0.5 mM, ▲ 1 mM, ▼ 10 mM, ◆ 100 mM.

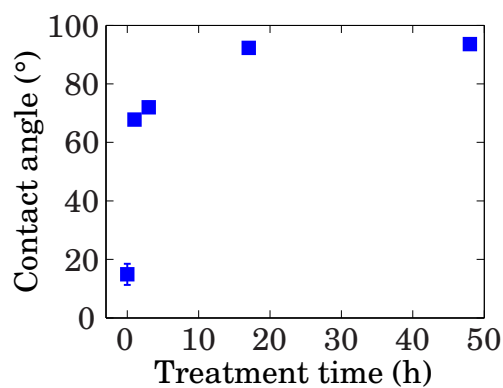


Figure 17: Water contact angle ($\pm 95\%$ CI) of CNF film as a function of time subjected to S6 vapour.

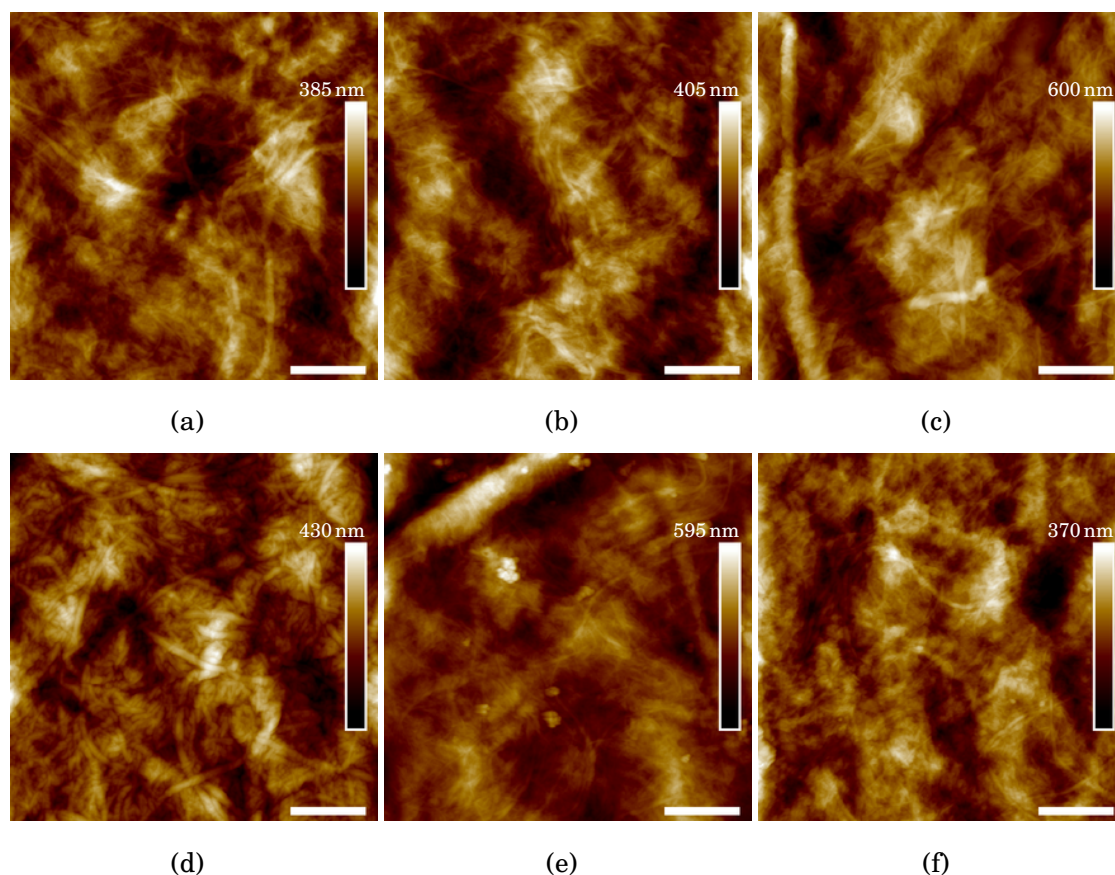


Figure 18: AFM height images of (a) the control sample and CNF films immersed in (b) S1 (100 mM), (c) S2 (100 mM), (d) S3 (0.1 mM), and (e) S6 (0.1 mM) for 17 h. (f) CNF film subjected to S6 vapour for 17 h. The scale bar represents 2 μm .

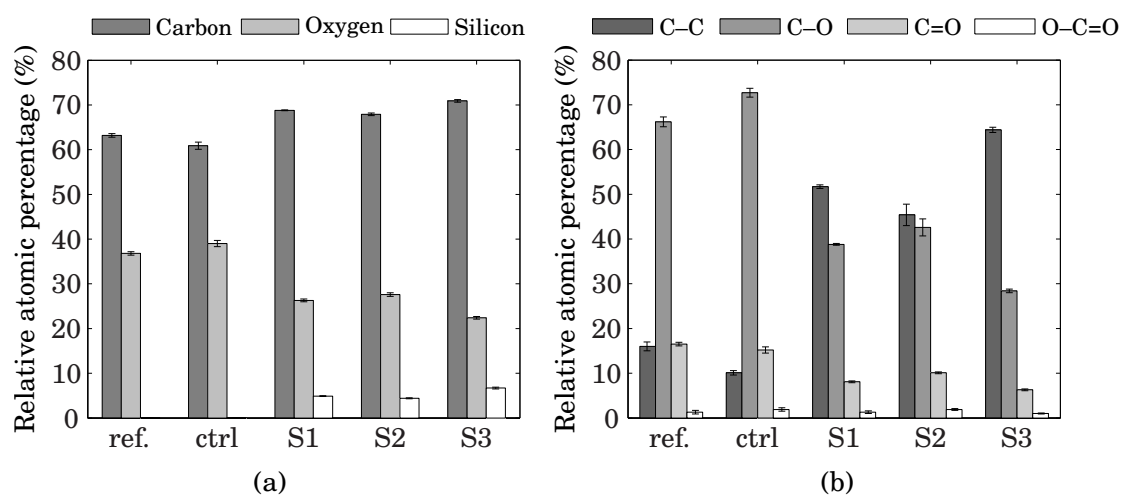


Figure 19: Relative atomic percentages ($\pm 95\%$ CI) of (a) carbon, oxygen, and silicon in the XPS survey spectra and (b) the components of high-resolution C 1s of reference, control, and silane-modified CNF films.

As a control sample, a native CNF film was immersed in toluene for 17 h after a 10 min UV/O₃ activation. The WCA didn't change significantly after drying the film overnight ($14.2^\circ \pm 1.2^\circ$), and similarly, AFM imaging indicated no apparent changes in the surface morphology of the film (Figure 18a). XPS analysis showed a smaller C–C component and a larger C–O component compared to the reference (Figure 18b), an indication of decreased contamination levels likely due to the UV/O₃ activation. Based on the above results, the growth recipes used in the stability tests were chosen as follows: 100 mM for S1 and S2, 0.1 mM for S3, each with 17 h immersion time. Comparing the kinetics data presented here with information found in literature is not straightforward as the substrates and chemicals vary greatly, but generally the requirement for higher concentration for silanes with fewer leaving groups, i.e. S1 and S2, is expected (Fadeev and McCarthy, 1999; Richter et al., 2000).

4.3 Stability

The results of the silane-modified CNF film stability tests introduced in Section 3.2.3 are presented next.

4.3.1 Ambient and Water Vapour

The WCA of silane-modified CNF films did not change markedly when stored in ambient environment for up to 8 wk or in 50 % RH for up to 4 wk (Figures 20a and 20b). Indications of the long-term ambient stability has been noted previously from studies on alkyltrichlorosilanes grown onto silicon, which showed stability for up to 18 months (Wasserman et al., 1989). Films treated with S1 and S2 show a decreasing trend in WCA initially when stored in 100 % RH (Figure 20c), while the last values (4 wk) indicate a negligible change with respect to the reference. This might be caused by condensed water drops that were seen on the films after 24 h and 1 wk experiments, giving them a more concentrated exposure to water. The data indicates further that S3-modified film retains its hydrophobic character at each time point. The stability of S3 is likely due to its ability to form highly cross-linked mono- and multilayers. This is in keeping with the good stability of longer alkyl chain silanes immersed in saline solution for 10 days (Wang et al., 2005). The WCA of the control film increased, which could be due to deposition of contaminants and their blocking of the native hydrophilic surface chemical groups.

The AFM images in Figure 22 illustrate the challenges of characterizing morphological changes occurring in the CNF film. The initial morphology contains fibrous and granular features and analysing the extent to which the stability tests affect the morphology is problematic, though some speculations can be made. The surface morphology and chemical composition of the control sample was left unaltered (Figures 22a, 22b, 22c, and 21), while XPS analysis revealed little change in the relative atomic percentages of carbon, oxygen, and silicon when the silane-modified films were stored 4 wk in 50 and 100 % RH, but changes after 8 wk in ambient

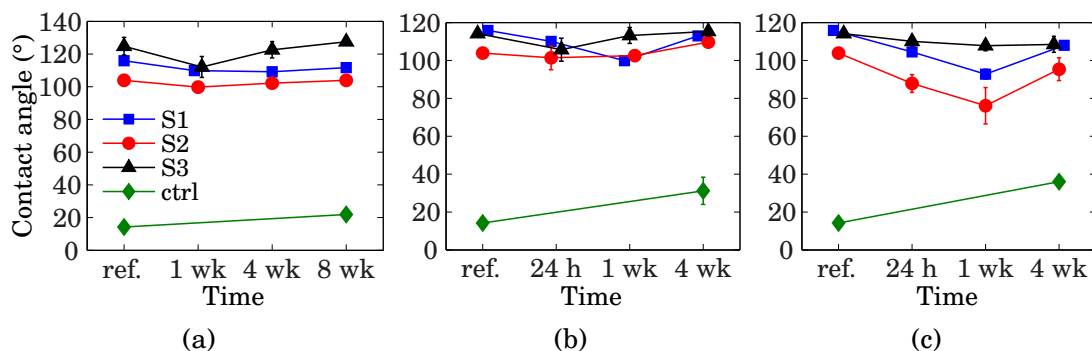


Figure 20: Water contact angle ($\pm 95\%$ CI) of control and silane-modified CNF films as a function of storage time in (a) ambient environment, (b) 50% RH, and (c) 100% RH.

conditions are clear and varied (Figure 21). S1-SAM undergoes a slight decrease in carbon and silicon, and an increase in oxygen, while the opposite behaviour is seen for S2 and S3. To some extent, these variations could be related to variations inherent to the silane treatment, e.g., the changes experienced by S3-modified film can be explained by the different growth modes that it exhibits. The monolayer and multilayer growth modes were not characterized in XPS separately, but the growth of S3 is clearly different in Figure 22j relative to Figures 22k and 22l. More silane translates to higher silicon and carbon with lower oxygen content. The increase in carbon percentage could at least partly result from an intake of carbonaceous contaminants. A quite drastic change occurred for S2-SAM; a much higher carbon content together with equal contribution from oxygen and silicon, while AFM imaging revealed highly shrouded morphology (Figure 22g). The conclusion must be held that contamination of unknown origin must have influenced these results.

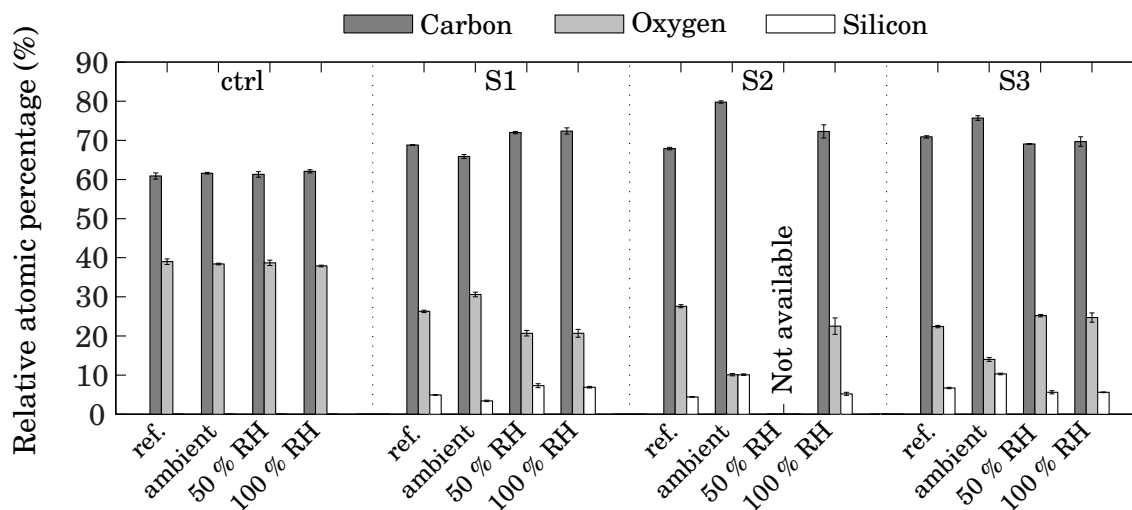


Figure 21: Relative atomic percentages of carbon, oxygen, and silicon in the XPS survey spectra of control and silane-modified CNF films after 8 wk in ambient, 4 wk in 50% RH, and 4 wk in 100% RH.

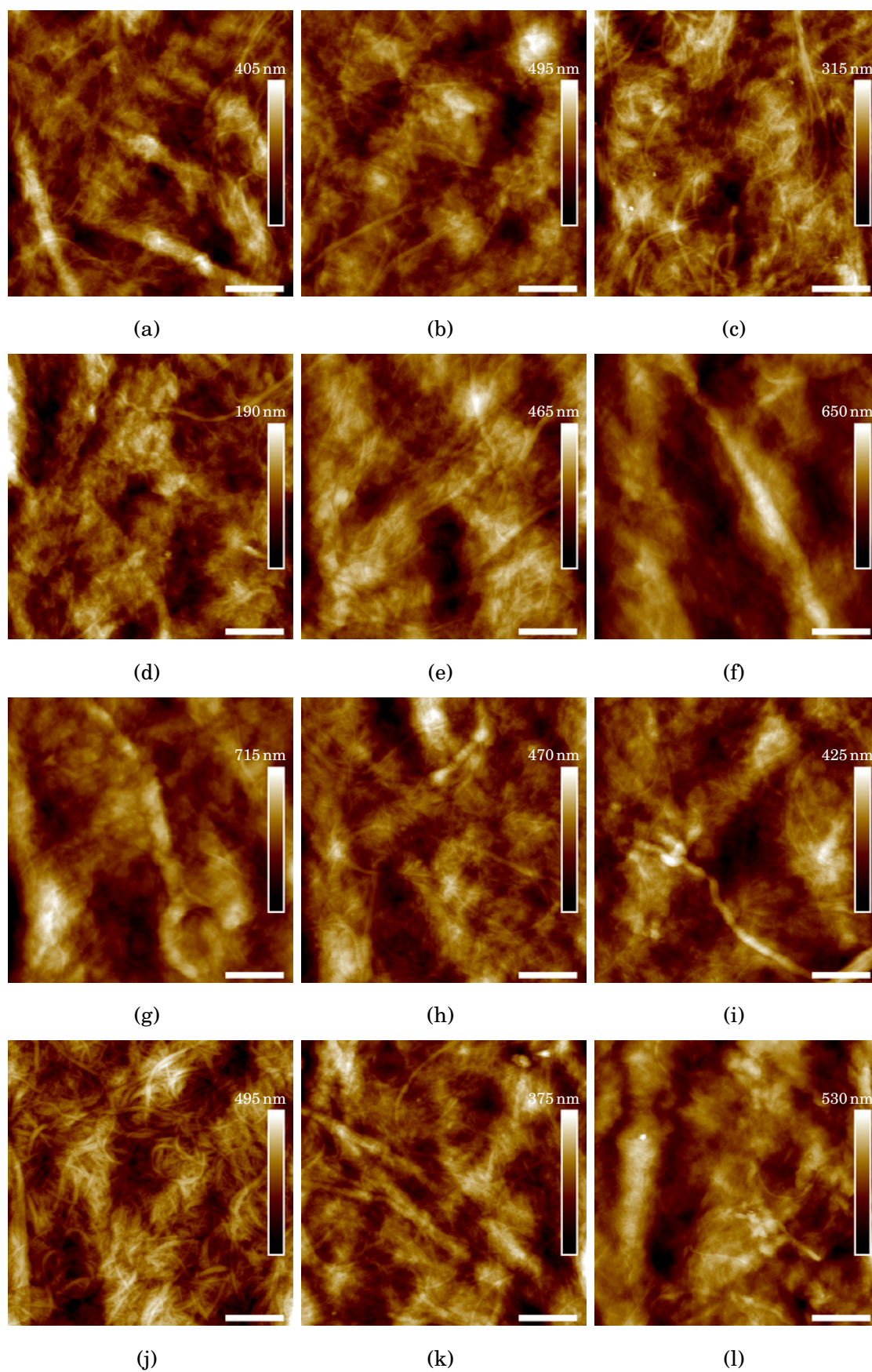


Figure 22: AFM height images of (a)–(c) the control sample, (d)–(f) S1, (g)–(i) S2, (j)–(l) S3-modified CNF films stored in ambient environment for 8 wk (first column), 50 % RH for 4 wk (second column), and 100 % RH for 4 wk (third column). The scale bar represents 2 μm.

4.3.2 HCl and NH₃ Vapour

After subjecting S1-modified CNF film to HCl or NH₃ vapour for 1 h, no significant change in WCA was observed in samples without a subsequent rinse and ones rinsed with acetone, while toluene rinse resulted in a moderate decrease (Figure 23). Due to these results, AFM imaging and XPS analysis were omitted. The ability of S1-SAM to resist the hydrolysis in acidic and alkaline conditions could result from the long hydrophobic alkyl chain and their dense packing, impeding the diffusion of water into the SAM-cellulose interface.

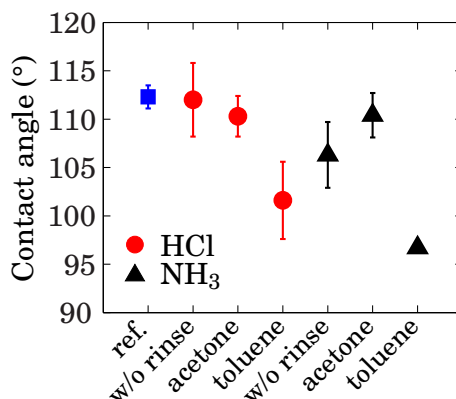


Figure 23: Water contact angle (\pm 95 % CI) of S1-modified CNF film after 1 h HCl or NH₃ vapour treatment. The horizontal axis lists the solvents used to rinse the film afterwards.

4.3.3 UV Light and UV/O₃

The WCA of S1-modified CNF film exposed to 254 nm and 366 nm wavelength UV light for 1 h did not change, thus the AFM and XPS analyses were omitted and the approach was not investigated further. The ineffectiveness of the chosen UV wavelengths to degrade the SAM is likely due to their insufficient wavelength needed to cleave C–C bonds and the absence of reactive oxygen species (Ye et al., 2001).

When the silane-modified films were subjected to UV light in conjunction with ozone, the WCA of S1 and S3 decreased below 20° after 30 min exposure, while for S2-SAM, the degradation was slightly slower (Figure 24a). The UV/O₃ treatment had no seeming effect on the surface morphology of the films (Figure 25). The XPS analysis shows that the C–C component decreases with increasing exposure time, while the relative percentages of oxidised groups, i.e. C–O, C=O, and O–C=O, increase as the degradation proceeds (Figures 24b and 26b). Figure 26a shows further that the relative atomic percentage of silicon does not disappear in the XPS survey spectra, indicating that the cellulose is left at least partly substituted with silicon. These results are in accordance with the studies of degradation kinetics by Ye et al. (2005).

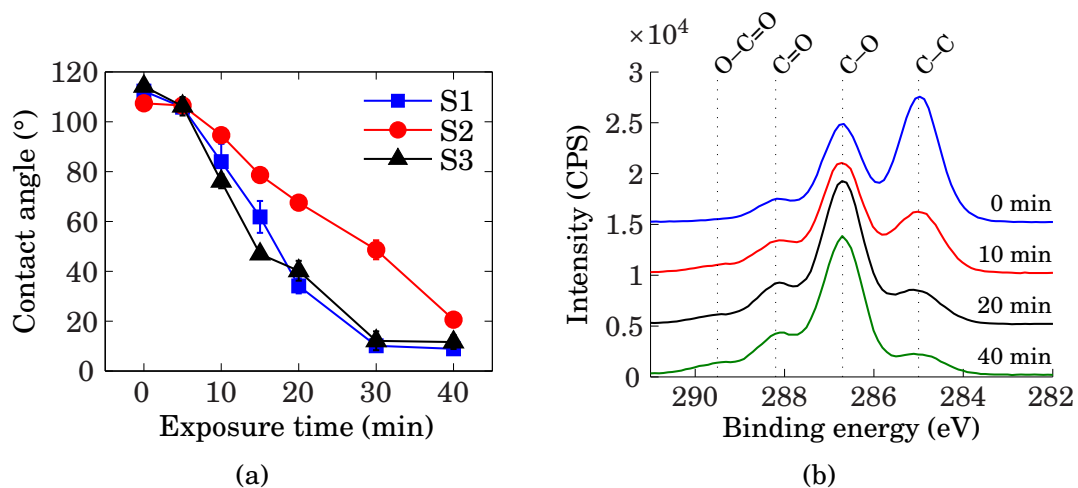


Figure 24: (a) Water contact angle ($\pm 95\%$ CI) of silane-modified CNF films as a function of UV/O₃ exposure time. (b) High-resolution C 1s XPS spectra of S1-modified CNF film exposed to UV/O₃ for 0, 10, 20, and 40 min.

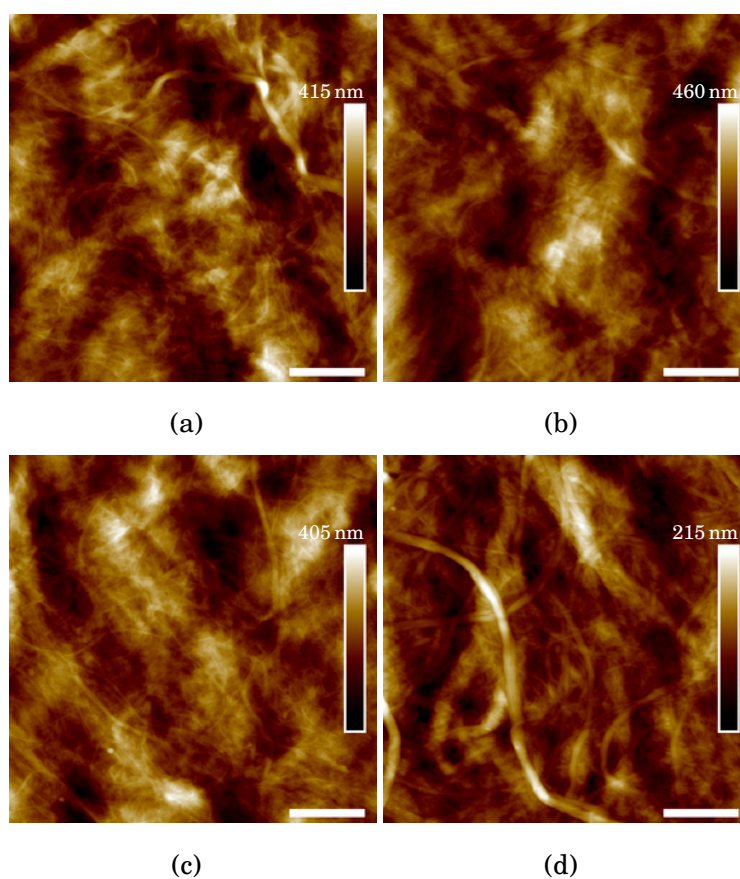
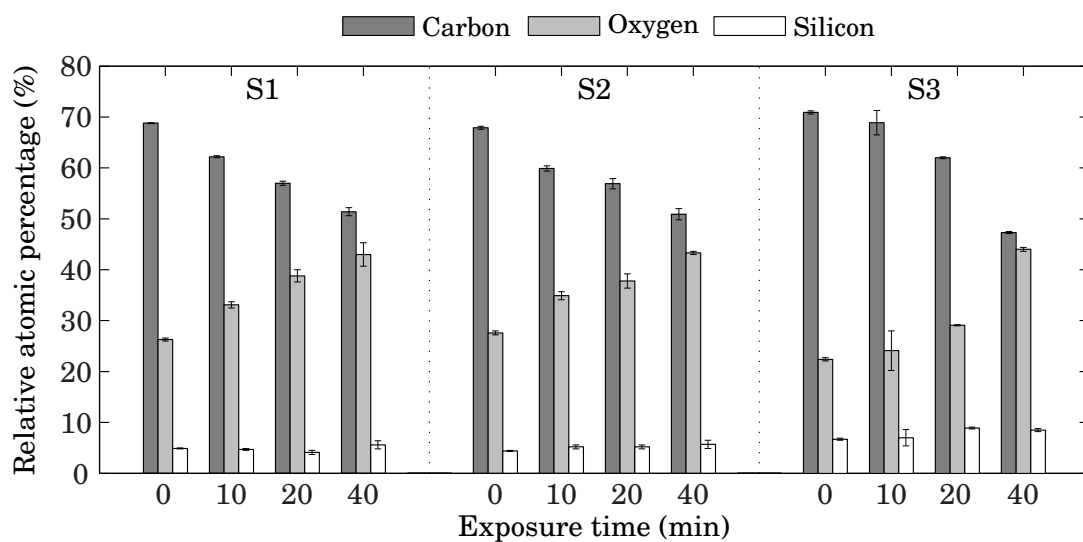
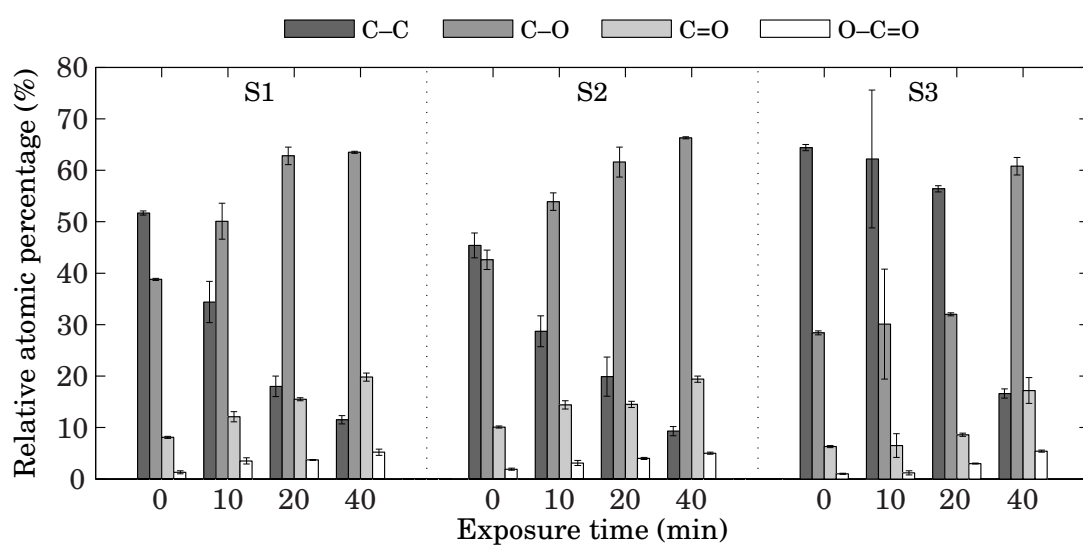


Figure 25: AFM height images of (a) S1, (b) S2, and (c) S3-modified CNF films exposed to UV/O₃ for 40 min. The scale bar represents 2 μm.



(a)



(b)

Figure 26: Relative atomic percentages ($\pm 95\%$ CI) of (a) carbon, oxygen, and silicon in the XPS survey spectra and (b) the components of high-resolution C 1s spectra (cf. Figure 24b) of silane-modified CNF films as a function of UV/O₃ exposure time.

4.4 Patterning of SAMs via Masked UV/O₃ Exposure

UV/O₃ exposure with a polydimethylsiloxane or metal mask was used to selectively degrade silane monolayers. Based on the WCA results of Figure 24a, 30 min exposure was used for S1 and S3, and 40 min for S2. The films were then rinsed with ca. 15 mL of toluene. The degraded areas were noticeably darker in shade (Figure 27), though this change in colour varied in magnitude between different silane treatment batches. The channels of the patterned SAM shown in Figure 27 did not noticeably wet or wick after placing a Milli-Q water droplet on the round pads. Only a bulge in the drop's surface was noticed at the site of a channel. It is possible that the substitution of hydroxyls with silanes takes place also on the buried fibrils of the CNF film. The UV/O₃ treatment most likely only degrades the silanes on the top of the film, leaving the buried fibrils hydrophobic, which together with the small pore size of CNF could affect the wetting and wicking behaviour of the channels.

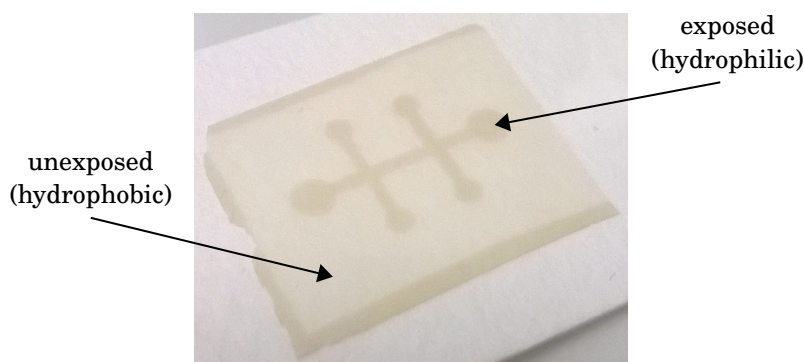


Figure 27: S1-modified CNF film after 30 min masked UV/O₃ exposure.

4.5 BSA and PEI Adsorption

Figure 28 shows the relative atomic percentage of nitrogen in the XPS survey spectra of CNF films subjected to BSA and PEI in buffered aqueous solutions. The amount of adsorbed BSA on native and UV/O₃-activated CNF films seems to be largely unaffected by the solution pH, whereas the hydrophobic S1-modified film and its UV/O₃-degraded counterpart show larger variation in BSA content. The increased hydrophilicity of UV/O₃-treated CNF film decreases the adsorption of BSA as expected (Ostuni et al., 2001), while the decrease of BSA content at pH 7 on UV/O₃-treated S1-SAM could be related to the crossing of pI, which is 4.7 for BSA (Malamud and Drysdale, 1978), rendering BSA cationic at pH 4 and anionic at pH 7. Besides other interactions, e.g. hydrogen bonding, this leads to an electrostatic attraction at pH 4 and repulsion at pH 7 between proteins and the anionic surface. The difference in BSA content of S1-SAM at the two pH can be explained by the difference in salt concentration of their respective solvents. PBS has a high salt

concentration, which creates a large screening effect and a more compact BSA conformation compared to AA. Less BSA can thus be adsorbed per unit area at pH 7. Also, BSA is likely more strongly anionic at pH 7 compared to its cationic strength at pH 4 (Tanford and Buzzell, 1956), causing larger repulsive forces between proteins and decreased adsorption at pH 7. Furthermore, the effect of hydrophobic interactions could be stronger at pH 4 due to partial unfolding of BSA (Wang et al., 2012).

The higher amounts of BSA on UV/O₃-treated S1-SAM compared to native CNF could be explained by a higher surface charge of the former surface, which requires larger amounts of adsorbed species to compensate the surface charge. The increase in surface charge could originate from the substitution of cellulose hydroxyl groups with the three alkyls of S1, leading to triple the amount of possible charge-bearing groups in an aqueous solution after UV ozonation (see Section 2.3.2).

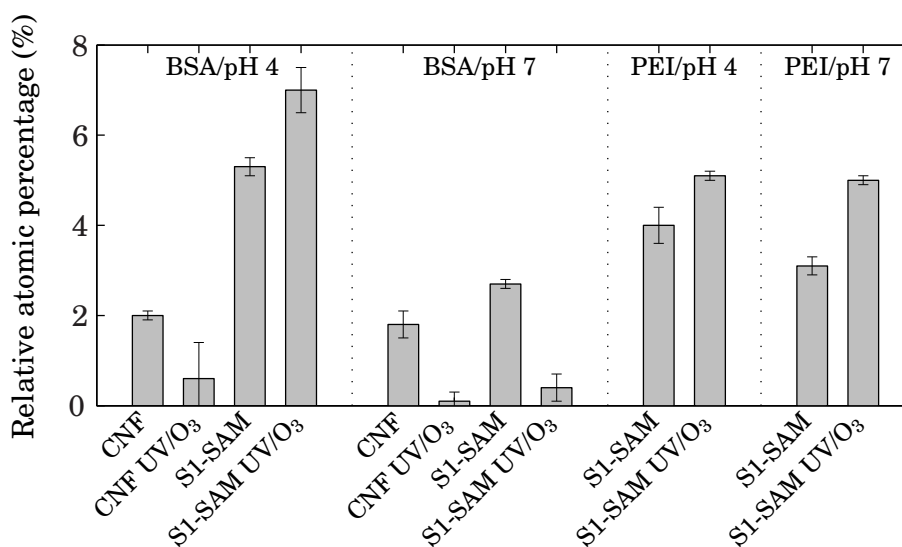


Figure 28: Relative atomic percentages ($\pm 95\%$ CI) of nitrogen in the XPS survey spectra of native and S1-modified CNF films immersed in aqueous BSA or PEI for 30 min: CNF = native CNF film, CNF UV/O₃ = CNF film UV/O₃-activated for 10 min, S1-SAM = S1-modified CNF film, and S1-SAM UV/O₃ = S1-modified CNF film UV-ozonated for 30 min.

The amount of adsorbed PEI on UV/O₃-treated S1-SAM is similar at both pH and somewhat larger compared to the S1-modified surface, which is likely to result from a strong electrostatic attraction between the cationic polymers and the anionic surface at both pH and the relatively weaker non-electrostatic attraction between PEI and S1-SAM, respectively. The notable PEI content on a hydrophobic surface and its only slight decrease at pH 7 could indicate that PEI adsorbs mainly non-electrostatically onto S1-SAM, as the decrease in PEI content of S1-SAM at pH 7 could be linked to the higher salt concentration of PBS, which diminishes electrostatic attraction between polymer segments and the surface, while not inhibiting the adsorption completely. (van de Steeg et al., 1992)

5 Conclusions

The growth of alkylsilane monolayers onto CNF film was studied. The film was rendered hydrophobic by the silane modification with no apparent effect on the surface morphology of the films for S1 and S2. With S3, a slight swelling of fibril features was noted that varied in magnitude, which is most likely related to the ability of S3 to cross-link and form multilayered films. Presence of silane-lumps was persistent in S6 treatment, and hence S6 was excluded from stability tests. XPS confirmed the presence of silicon and aliphatic carbon species, which together with the increased WCA is an indicative of a successful chemisorption of silanes onto the cellulosic substrate.

The silane-modification was shown to be stable in ambient conditions for up to 8 wk and in 50 % RH up to 4 wk. The decrease in WCA in acidic and alkaline vapours was slow probably due to defect-driven kinetics and the large hydrophobic component of the monolayer acting as an effective water diffusion barrier. The two in-house UV lamps failed to change the wetting characteristics of the S1-modified CNF film. UV light in conjunction with reactive oxygen species was used successfully to degrade the alkyl chains, leaving oxidised silicon groups attached to the film. The method was further used to create hydrophilic-hydrophobic patterns on the film surface by masking the exposure with a polymer or metal mask. The channels turned out to be too narrow to be wetted, and concerns over the necessary depth of UV/O₃-removal was put into question along with the wicking of native and silane-modified films. BSA adsorption onto CNF from buffered aqueous solutions indicated a contrast for selective adsorption with respect to native and UV/O₃-activated CNF, and also with S1-modified film and UV/O₃-degraded S1-SAM.

In conclusion, the application of CNF film as a substrate for controlled fluid transport was not achieved and further inquiries into spatial placement of alkylsilanes in the film needs to be addressed to provide insight into its wicking behaviour. Nevertheless, the CNF film offers a smooth chemically homogeneous platform with good and manageable rigidity when exposed to non-aqueous and aqueous solvents, respectively, although quantifying morphological changes might prove occasionally challenging.

References

- AALTO.FI (2014). Sustainability at Aalto University. <http://www.aalto.fi/en/about/strategy/sustainability/> (accessed 17.8.2014).
- APILUX, A., UKITA, Y., CHIKAE, M., CHAILAPAKUL, O., and TAKAMURA, Y. (2013). Development of automated paper-based devices for sequential multistep sandwich enzyme-linked immunosorbent assays using inkjet printing. *Lab on a Chip*, 13(1):126–135.
- ARKLES, B. (1977). Tailoring surfaces with silanes. *Chemtech*, 7(12):766–778.
- ARKLES, B. (2006). Hydrophobicity, hydrophilicity and silanes. *Paint and Coatings Industry*, 22(10):114–135.
- BEAR, J. (1988). *Dynamics of fluids in porous media*. Dover.
- BIGELOW, W. C., PICKETT, D. L., and ZISMAN, W. A. (1946). Oleophobic monolayers: I. Films adsorbed from solution in non-polar liquids. *Journal of Colloid Science*, 1(6):513–538.
- BLOW, N. (2009). Microfluidics: The great divide. *Nature Methods*, 6(9):683–686.
- BRANDRISS, S. and MARGEL, S. (1993). Synthesis and characterization of self-assembled hydrophobic monolayer coatings on silica colloids. *Langmuir*, 9(5):1232–1240.
- BUCHHOLZ, V., WEGNER, G., STEMME, S., and ÖDBERG, L. (1996). Regeneration, derivatization and utilization of cellulose in ultrathin films. *Advanced Materials*, 8(5):399–402.
- BUTT, H.-J., GRAF, K., and KAPPL, M. (2003). *Physics and chemistry of interfaces*. John Wiley & Sons, Inc.
- CARRILHO, E., MARTINEZ, A. W., and WHITESIDES, G. M. (2009). Understanding wax printing: A simple micropatterning process for paper-based microfluidics. *Analytical Chemistry*, 81(16):7091–7095.
- CASSIE, A. B. D. and BAXTER, S. (1944). Wettability of porous surfaces. *Transactions of the Faraday Society*, 40:546–551.
- CHANDEKAR, A., SENGUPTA, S. K., and WHITTEN, J. E. (2010). Thermal stability of thiol and silane monolayers: A comparative study. *Applied Surface Science*, 256(9):2742–2749.
- CHANDLER, D. (2005). Interfaces and the driving force of hydrophobic assembly. *Nature*, 437(7059):640–647.
- CHAPMAN, R. G., OSTUNI, E., TAKAYAMA, S., HOLMLIN, R. E., YAN, L., and WHITESIDES, G. M. (2000). Surveying for surfaces that resist the adsorption of proteins. *Journal of the American Chemical Society*, 122(34):8303–8304.

- COMMISSION REGULATION (2011). Amending Annex II to Regulation (EC) No 1333/2008 of the European Parliament and of the Council by establishing a Union list of food additives. *Official Journal of the European Union*, L 295.
- DEMORE, W. B., SANDER, S. P., GOLDEN, D. M., HAMPSON, R. F., KURYLO, M. J., HOWARD, C. J., RAVISHANKARA, A. R., KOLB, C. E., and MOLINA, M. J. (1997). Chemical kinetics and photochemical data for use in stratospheric modeling. *National Aeronautics and Space Administration, Jet Propulsion Laboratory, California Institute of Technology*, JPL Publication 97-4.
- DING, S.-Y. and HIMMEL, M. E. (2006). The maize primary cell wall microfibril: A new model derived from direct visualization. *Journal of Agricultural and Food Chemistry*, 54(3):597–606.
- DULCEY, C. S., GEORGER JR., J. H., KRAUTHAMER, V., STENGER, D. A., FARE, T. L., and CALVERT, J. M. (1991). Deep UV photochemistry of chemisorbed monolayers: Patterned coplanar molecular assemblies. *Science*, 252(5005):551–554.
- DÉJARDIN, P. (editor) (2006). *Proteins at solid-liquid interfaces*. Springer.
- FADEEV, A. Y. and MCCARTHY, T. J. (1999). Trialkylsilane monolayers covalently attached to silicon surfaces: Wettability studies indicating that molecular topography contributes to contact angle hysteresis. *Langmuir*, 15(11):3759–3766.
- FADEEV, A. Y. and MCCARTHY, T. J. (2000). Self-assembly is not the only reaction possible between alkyltrichlorosilanes and surfaces: Monomolecular and oligomeric covalently attached layers of dichloro- and trichloroalkylsilanes on silicon. *Langmuir*, 16(18):7268–7274.
- FENTON, E. M., MASCARENAS, M. R., LÓPEZ, G. P., and SIBBETT, S. S. (2009). Multiplex lateral-flow test strips fabricated by two-dimensional shaping. *ACS Applied Materials and Interfaces*, 1(1):124–129.
- FOBEL, R., KIRBY, A. E., NG, A. H. C., FARNOOD, R. R., and WHEELER, A. R. (2014). Paper microfluidics goes digital. *Advanced Materials*, 26(18):2838–2843.
- FU, E., LUTZ, B., KAUFFMAN, P., and YAGER, P. (2010). Controlled reagent transport in disposable 2D paper networks. *Lab on a Chip*, 10(7):918–920.
- GAO, L. and MCCARTHY, T. J. (2006). Contact angle hysteresis explained. *Langmuir*, 22(14):6234–6237.
- GAO, L. and MCCARTHY, T. J. (2007). How Wenzel and Cassie were wrong. *Langmuir*, 23(7):3762–3765.
- HAUGSTAD, G. (2012). *Atomic force microscopy: Understanding basic modes and advanced applications*. John Wiley & Sons, Inc.
- HENCH, L. L. and WEST, J. K. (1990). The sol-gel process. *Chemical Reviews*, 90(1):33–72.

- HON, D. N.-S. and SHIRAISHI, N. (2000). *Wood and cellulosic chemistry, 2nd edition*. CRC Press.
- JOHANSSON, L.-S. (2002). Monitoring fibre surfaces with XPS in papermaking processes. *Microchimica Acta*, 138(3–4):217–223.
- JUNCKER, D., SCHMID, H., DRECHSLER, U., WOLF, H., WOLF, M., MICHEL, B., DE ROOIJ, N., and DELAMARCHE, E. (2002). Autonomous microfluidic capillary system. *Analytical Chemistry*, 74(24):6139–6144.
- KLASNER, S. A., PRICE, A. K., HOEMAN, K. W., WILSON, R. S., BELL, K. J., and CULBERTSON, C. T. (2010). Paper-based microfluidic devices for analysis of clinically relevant analytes present in urine and saliva. *Analytical and Bioanalytical Chemistry*, 397(5):1821–1829.
- KLEMM, D., HEUBLEIN, B., FINK, H.-P., and BOHN, A. (2005). Cellulose: Fascinating biopolymer and sustainable raw material. *Angewandte Chemie International Edition*, 44(22):3358–3393.
- KLEMM, D., KRAMER, F., MORITZ, S., LINDSTRÖM, T., ANKERFORS, M., GRAY, D., and DORRIS, A. (2011). Nanocelluloses: A new family of nature-based materials. *Angewandte Chemie International Edition*, 50(24):5438–5466.
- KLUTH, G. J., SUNG, M. M., and MABOUDIAN, R. (1997). Thermal behavior of alkylsiloxane self-assembled monolayers on the oxidized Si(100) surface. *Langmuir*, 13(14):3775–3780.
- KONTTURI, E., THÜNE, P. C., ALEXEEV, A., and NIEMANTSVERDRIET, J. W. (2005). Introducing open films of nanosized cellulose—atomic force microscopy and quantification of morphology. *Polymer*, 46(10):3307–3317.
- LANDAU, L. D. and LIFSHITZ, E. M. (1987). *Fluid mechanics, 2nd edition*. Butterworth-Heinemann.
- LANGMUIR, I. (1920). The mechanism of the surface phenomena of flotation. *Transactions of the Faraday Society*, 15:62–74.
- LI, X., BALLERINI, D. R., and SHEN, W. (2012). A perspective on paper-based microfluidics: Current status and future trends. *Biomicrofluidics*, 6(1):011301.
- LI, X., TIAN, J., GARNIER, G., and SHEN, W. (2010). Fabrication of paper-based microfluidic sensors by printing. *Colloids and Surfaces B: Biointerfaces*, 76(2):564–570.
- MALAMUD, D. and DRYSDALE, J. W. (1978). Isoelectric points of proteins: A table. *Analytical Biochemistry*, 86(2):620–647.
- MARMUR, A. (2006). Soft contact: Measurement and interpretation of contact angles. *Soft Matter*, 2(1):12–17.
- MARTINEZ, A. W., PHILLIPS, S. T., and WHITESIDES, G. M. (2008a). Three-dimensional microfluidic devices fabricated in layered paper and tape. *Pro-*

- ceedings of the National Academy of Sciences of the United States of America*, 105(50):19606–19611.
- MARTINEZ, A. W., PHILLIPS, S. T., WILEY, B. J., GUPTA, M., and WHITESIDES, G. M. (2008b). FLASH: A rapid method for prototyping paper-based microfluidic devices. *Lab on a Chip*, 8(12):2146–2150.
- MASOODI, R. and PILLAI, K. M. (2010). Darcy’s law-based model for wicking in paper-like swelling porous media. *AIChE Journal*, 56(9):2257–2267.
- MCGOVERN, M. E., KALLURY, K. M. R., and THOMPSON, M. (1994). Role of solvent on the silanization of glass with octadecyltrichlorosilane. *Langmuir*, 10(10):3607–3614.
- MILANEZ, D. H., AMARAL, R. M., FARIA, L. I. L., and GREGOLIN, J. A. R. (2013). Assessing nanocellulose developments using science and technology indicators. *Materials Research*, 16(3):635–641.
- MOHITE, B. V. and PATIL, S. V. (2014). A novel biomaterial: Bacterial cellulose and its new era applications. *Biotechnology and Applied Biochemistry*, 61(2):101–110.
- NAKASHIMA, Y. and YASUDA, T. (2007). Cell differentiation guidance using chemical stimulation controlled by a microfluidic device. *Sensors and Actuators, A: Physical*, 139(1–2):252–258.
- NORDE, W. and ZOUNGRANA, T. (1998). Surface-induced changes in the structure and activity of enzymes physically immobilized at solid/liquid interfaces. *Biotechnology and Applied Biochemistry*, 28(2):133–143.
- ORNATSKA, M., SHARPE, E., ANDREESCU, D., and ANDREESCU, S. (2011). Paper bioassay based on ceria nanoparticles as colorimetric probes. *Analytical Chemistry*, 83(11):4273–4280.
- OSBORN, J. L., LUTZ, B., FU, E., KAUFFMAN, P., STEVENS, D. Y., and YAGER, P. (2010). Microfluidics without pumps: Reinventing the T-sensor and H-filter in paper networks. *Lab on a Chip*, 10(20):2659–2665.
- OSTUNI, E., CHAPMAN, R. G., HOLMLIN, R. E., TAKAYAMA, S., and WHITESIDES, G. W. (2001). A survey of structure-property relationships of surfaces that resist the adsorption of protein. *Langmuir*, 17(18):5605–5620.
- PELLERITE, M. J., WOOD, E. J., and JONES, V. W. (2002). Dynamic contact angle studies of self-assembled thin films from fluorinated alkyltrichlorosilanes. *Journal of Physical Chemistry B*, 106(18):4746–4754.
- PLACKETT, D. (editor) (2011). *Biopolymers: New materials for sustainable films and coatings*. John Wiley & Sons, Inc.
- PÄÄKKÖ, M., ANKERFORS, M., KOSONEN, H., NYKÄNEN, A., AHOLA, S., ÖSTERBERG, M., RUOKOLAINEN, J., LAINE, J., LARSSON, P. T., IKKALA, O., and

- LINDSTRÖM, T. (2007). Enzymatic hydrolysis combined with mechanical shearing and high-pressure homogenization for nanoscale cellulose fibrils and strong gels. *Biomacromolecules*, 8(6):1934–1941.
- REICHL, L. E. (2009). *A modern course in statistical physics*. John Wiley & Sons, Inc.
- RICHTER, A. G., YU, C. ., DATTA, A., KMETKO, J., and DUTTA, P. (2000). In situ and interrupted-growth studies of the self-assembly of octadecyltrichlorosilane monolayers. *Physical Review E: Statistical Physics, Plasmas, Fluids, and Related Interdisciplinary Topics*, 61(1):607–615.
- SCHREIBER, F. (2000). Structure and growth of self-assembling monolayers. *Progress in Surface Science*, 65(5–8):151–256.
- SIMONEIT, B. R. T. (2002). Biomass burning—a review of organic tracers for smoke from incomplete combustion. *Applied Geochemistry*, 17(3):129–162.
- SMOOK, G. A. (1992). *Handbook for pulp & paper technologists, 2nd edition*. Angus Wilde Publications.
- SRINIVASAN, U., HOUSTON, M. R., HOWE, R. T., and MABOUDIAN, R. (1998). Alkyltrichlorosilane-based self-assembled monolayer films for stiction reduction in silicon micromachines. *Journal of Microelectromechanical Systems*, 7(2):252–259.
- STEVENS, M. J. (1999). Thoughts on the structure of alkylsilane monolayers. *Langmuir*, 15(8):2773–2778.
- STRYER, L. (1995). *Biochemistry, 4th edition*. W.H. Freeman and Company.
- SUGIMURA, H., HOZUMI, A., KAMEYAMA, T., and TAKAI, O. (2002). Organosilane self-assembled monolayers formed at the vapour/solid interface. *Surface and Interface Analysis*, 34(1):550–554.
- SUGIMURA, H., USHIYAMA, K., HOZUMI, A., and TAKAI, O. (2000). Micropatterning of alkyl- and fluoroalkylsilane self-assembled monolayers using vacuum ultraviolet light. *Langmuir*, 16(3):885–888.
- SWAIN, P. S. and LIPOWSKY, R. (1998). Contact angle on heterogeneous surfaces: A new look at Cassie’s and Wenzel’s laws. *Langmuir*, 14(23):6772–6780.
- TANFORD, C. and BUZZELL, J. G. (1956). The viscosity of aqueous solutions of bovine serum albumin between pH 4.3 and 10.5. *Journal of Physical Chemistry*, 60(2):225–231.
- TEKES.FI (2014). Tekes ongoing programmes. <http://www.tekes.fi/en/programmes-and-services/tekes-programmes/> (accessed 17.8.2014).
- TRIPP, C. P. and HAIR, M. L. (1995). Reaction of methylsilanols with hydrated silica surfaces: The hydrolysis of trichloro-, dichloro-, and monochloromethylsilanes and the effects of curing. *Langmuir*, 11(1):149–155.

- TURYAN, I. and MANDLER, D. (1997). Selective determination of Cr(VI) by a self-assembled monolayer-based electrode. *Analytical Chemistry*, 69(5):894–897.
- ULMAN, A. (1996). Formation and structure of self-assembled monolayers. *Chemical Reviews*, 96(4):1533–1554.
- VALTIONEUVOSTO.FI (2013). Valtioneuvoston periaatepäätös kestävien ympäristö- ja energiaratkaisujen (cleantech-ratkaisut) edistämisestä julkisissa hankinnoissa. <http://valtioneuvosto.fi/toiminta/periaatepaatokset/periaatepaatos/fi.jsp?oid=388513> (accessed 18.8.2014). Valtioneuvoston periaatepäätös Kestävän kulutuksen ja tuotannon ohjelmasta Vähemmästä viisaammin. <http://valtioneuvosto.fi/toiminta/periaatepaatokset/periaatepaatos/fi.jsp?oid=388570> (accessed 18.8.2014).
- VAN DE STEEG, H. G. M., STUART, M. A. C., DE KEIZER, A., and BIJSTERBOSCH, B. H. (1992). Polyelectrolyte adsorption: A subtle balance of forces. *Langmuir*, 8(10):2538–2546.
- VAN DER HEIDE, P. (2012). *X-ray photoelectron spectroscopy: An introduction to principles and practices*. John Wiley & Sons, Inc.
- WANG, A., TANG, H., CAO, T., SALLEY, S. O., and NG, K. Y. S. (2005). In vitro stability study of organosilane self-assemble monolayers and multilayers. *Journal of Colloid and Interface Science*, 291(2):438–447.
- WANG, X., LIU, G., and ZHANG, G. (2012). Effect of surface wettability on ion-specific protein adsorption. *Langmuir*, 28(41):14642–14653.
- WASSERMAN, S. R., WHITESIDES, G. M., TIDSWELL, I. M., OCKO, B. M., PERSHAN, P. S., and AXE, J. D. (1989). The structure of self-assembled monolayers of alkylsiloxanes on silicon: A comparison of results from ellipsometry and low-angle X-ray reflectivity. *Journal of the American Chemical Society*, 111(15):5852–5861.
- WEI, T., KAEWTATHIP, S., and SHING, K. (2009). Buffer effect on protein adsorption at liquid/solid interface. *Journal of Physical Chemistry C*, 113(6):2053–2062.
- WENZEL, R. N. (1936). Resistance of solid surfaces to wetting by water. *Journal of Industrial & Engineering Chemistry*, 28(8):988–994.
- WHITESIDES, G. M. (2006). The origins and the future of microfluidics. *Nature*, 442(7101):368–373.
- WHITESIDES, G. M. and GRZYBOWSKI, B. (2002). Self-assembly at all scales. *Science*, 295(5564):2418–2421.
- WHYMAN, G., BORMASHENKO, E., and STEIN, T. (2008). The rigorous derivation of Young, Cassie-Baxter and Wenzel equations and the analysis of the contact angle hysteresis phenomenon. *Chemical Physics Letters*, 450(4–6):355–359.

- WWF.PANDA.ORG (2014). WWF: History, people, operations. http://wwf.panda.org/who_we_are/ (accessed 25.8.2014).
- WÄGGER, L. (2000). Polyelectrolyte adsorption onto cellulose fibres—a review. *Nordic Pulp and Paper Research Journal*, 15(5):586–597.
- YE, T., MCARTHUR, E. A., and BORGUET, E. (2005). Mechanism of UV photoreactivity of alkylsiloxane self-assembled monolayers. *Journal of Physical Chemistry B*, 109(20):9927–9938.
- YE, T., WYNN, D., DUDEK, R., and BORGUET, E. (2001). Photoreactivity of alkylsiloxane self-assembled monolayers on silicon oxide surfaces. *Langmuir*, 17(15):4497–4500.
- YETISEN, A. K., AKRAM, M. S., and LOWE, C. R. (2013). Paper-based microfluidic point-of-care diagnostic devices. *Lab on a Chip*, 13(12):2210–2251.
- YOUNG, T. (1805). An essay on the cohesion of fluids. *Philosophical Transactions of the Royal Society of London*, 95:65–87.
- YOUNGBLOOD, J. P. and MCCARTHY, T. J. (1999). Ultrahydrophobic polymer surfaces prepared by simultaneous ablation of polypropylene and sputtering of poly(tetrafluoroethylene) using radio frequency plasma. *Macromolecules*, 32(20):6800–6806.
- ZHANG, F., SKODA, M. W. A., JACOBS, R. M. J., MARTIN, R. A., MARTIN, C. M., and SCHREIBER, F. (2007). Protein interactions studied by SAXS: Effect of ionic strength and protein concentration for BSA in aqueous solutions. *Journal of Physical Chemistry B*, 111(1):251–259.
- ZHANG, S. (2003). Fabrication of novel biomaterials through molecular self-assembly. *Nature Biotechnology*, 21(10):1171–1178.
- ZHUANG, Y. X., HANSEN, O., KNIELING, T., WANG, C., ROMBACH, P., LANG, W., BENECKE, W., KEHLENBECK, M., and KOBLITZ, J. (2006). Thermal stability of vapor phase deposited self-assembled monolayers for MEMS anti-stiction. *Journal of Micromechanics and Microengineering*, 16(11):2259–2264.
- ÖSTERBERG, M., PERESIN, M. S., JOHANSSON, L.-S., and TAMMELIN, T. (2013a). Clean and reactive nanostructured cellulose surface. *Cellulose*, 20(3):983–990.
- ÖSTERBERG, M., VARTIAINEN, J., LUCENIUS, J., HIPPI, U., SEPPÄLÄ, J., SERIMAA, R., and LAINE, J. (2013b). A fast method to produce strong NFC films as a platform for barrier and functional materials. *ACS Applied Materials and Interfaces*, 5(11):4640–4647.